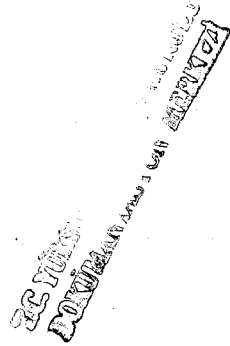


**CIRCULAR DELAMINATION EFFECTS ON
BUCKLING BEHAVIOUR OF THE LAMINATED
COMPOSITE PLATES WITH CIRCULAR HOLE**

A Thesis Submitted to the
Graduate School of Natural and Applied Sciences of
Dokuz Eylül University
In Partial Fulfillment of the Requirements for
the Degree of Master of Science in Mechanical Engineering, Mechanics
Program

738868

by
Yusuf ARMAN

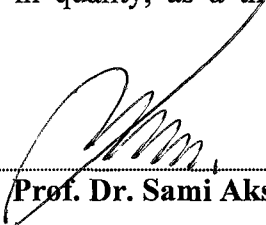


132868

June, 2003
İZMİR

Ms. Sc. THESIS EXAMINATION RESULT FORM

We certify that we have read the thesis, entitled “**CIRCULAR DELAMINATION EFFECTS ON BUCKLING BEHAVIOUR OF THE LAMINATED COMPOSITE PLATES WITH CIRCULAR HOLE**” completed by **YUSUF ARMAN** under supervision of **Prof. Dr. SAMİ AKSOY** and that in our opinion it is fully adequate, in scope and in quality, as a thesis for the degree of Master of Science.


Prof. Dr. Sami Aksoy

Supervisor


Prof. Dr. Ramazan Karakuzu

Committee Member


Assistant Prof. Dr. Hasan Yıldız

Committee Member

Approved by the
Graduate School of Natural and Applied Sciences


Prof. Dr. Cahit Helvacı

Director

ACKNOWLEDGEMENTS

I would like to express to my sincere gratitude to my supervisor, Prof. Dr. Sami AKSOY, for his excellent guidance and continuous encouragement throughout the preparation of this study.

I also would like to thank Prof. Dr. Onur SAYMAN, Prof. Dr. Ramazan KARAKUZU and Associate Prof. Dr. Mehmet ZOR for their academic support and encouragement through my M.Sc program.

I wish to express my thanks to my friends at the Department of Mechanical Engineering for their help and patience.

I also wish to thanks Ahmet YİĞİT, the technician in the Machine Tool Laboratory of the Mechanical Engineering Department.

Thanks go out to Izoreel Composite Isolate Materials Company and Mr. Rahmi AKIN for their help during production of the composite.

Finally, I am deeply indebted to my family for their support, patience and understanding throughout my life.

Yusuf ARMAN

ABSTRACT

In this study, the critical buckling loads depend on the delamination diameter around the hole and fiber rotation angles of the layers have been investigated in the rectangular laminated composite plates which have the circular hole in the centre and the circular delamination around the hole. In this investigation, the plate has been clamped from the two edges and the loaded uniaxially from the clamped edges. This investigation has been performed numerically and experimentally.

The prepared laminated composite plates for the experimental studies have been become from eight layers (four symmetric layers). In the layers, woven glass fiber as fiber and epoxy as resin have been used. The width of the plates is 200 mm, the height of the plates is 160 mm and the thickness of the plates is 1,6 mm and the plates have a hole whose diameter is $\varnothing_1=40$ mm in the centre. The delamination diameter of these plates which have single delamination in the centre of the layers changes as $\varnothing_2=0$ mm (without delamination), $\varnothing_2=80$ mm, $\varnothing_2=120$ mm and $\varnothing_2=160$ mm. In the experimental studies, the loading has been applied only in the direction of 0 degree $[0^\circ]$ fiber orientation angle.

Also for the numerical studies, three dimensional (3D) finite elements models which have a hole whose diameter is $\varnothing_1=40$ mm in the centre and the different delamination sizes in the centre of the layers have been established with assistance of ANSYS 6.1 finite element analysis program. Also, to investigate to the effect of the fiber orientation angle change, $[0^\circ]_s$, $[15^\circ]_s$, $[30^\circ]_s$ and $[45^\circ]_s$ fiber orientations have been analyzed.

In this study, firstly, the comparison between experimentally results which were obtained from the prepared test specimens and numerical results of these test

specimens has been done. Then, it has been seen that a good agreement between experimental results which were obtained and numerical results and in addition the numerical buckling load results of the other finite elements models which have different delamination diameters and different fiber orientation angles have been obtained.

Finally of all of the numerical and experimental studies, it has been seen that the different fiber orientation angles affected the critical buckling loads and the important decreases in the critical buckling loads were occurred after a certain value of the delamination diameter.



ÖZET

Bu çalışmada, ortasında dairesel delik ve delik etrafında dairesel delaminasyon bulunan dikdörtgen biçimindeki tabakalı kompozit plaklarda delik etrafındaki delaminasyon çapına ve tabakaların fiber yönlenme açılarına bağlı olarak kritik burkulma yükleri incelenmiştir. Bu incelemede plak iki kenarından ankastre olarak mesnetlenmiş ve ankastre kenarlardan tek eksenli olarak yüklenmiştir. Bu araştırma nümerik ve deneysel olarak yapılmıştır.

Deneysel çalışmalar için hazırlanan tabakalı kompozit plaklar, sekiz tabakadan (dört simetrik tabakadan) oluşmaktadır. Tabakalarda fiber olarak örgülü cam lifi ve reçine olarak da epoxy kullanılmıştır. Bu plakların genişliği 200 mm, yüksekliği 160 mm ve kalınlığı 1,6 mm olup ortalarında çapı $\varnothing_1=40$ mm olan bir deliğe sahiptirler. Tabakaların tam ortasında tek bir dairesel delaminasyona sahip olan bu plakların delaminasyon çapları sırasıyla $\varnothing_2=0$ mm (delaminasyonsuz), $\varnothing_2=80$ mm, $\varnothing_2=120$ mm ve $\varnothing_2=160$ mm olarak değişmektedir. Deneysel çalışmalarda sadece sıfır derece $[0^\circ]$ fiber yönlenme açısı yönünde yükleme yapılmıştır.

Nümerik çalışmalar için ise, ANSYS 6.1 sonlu elemanlar programı yardımı ile $200 \times 160 \times 1,6$ mm boyutlarındaki tabakalı kompozit plakların, ortalarında $\varnothing_1=40$ mm çapında bir deliğe ve tabakaların tam ortasında farklı delaminasyon çaplarına sahip 3 boyutlu sonlu elemanlar modelleri kurulmuştur. Fiber yönlenme açısının etkisini incelemek amacıyla da, tabakalara, sırasıyla $[0^\circ]_s$, $[15^\circ]_s$, $[30^\circ]_s$ ve $[45^\circ]_s$ fiber yönlenme açıları tanımlanmıştır.

Bu çalışmada, ilk olarak, hazırlanan deney numunelerinden elde edilen deneysel sonuçlar ile bu deney numunelerinin nümerik sonuçları arasındaki uyum araştırılmıştır. Daha sonra, elde edilen deneysel sonuçlar ile nümerik sonuçlar

arasında iyi bir uyum olduđu gözlenmiş ve ilave olarak farklı delaminasyon çaplarına ve farklı fiber yönlenme açalarına sahip diđer sonlu elemanlar modellerinin nümerik burkulma yükü sonuçları elde edilmiştir.

Bütün bu deneysel ve nümerik çalışmaların sonucunda, kritik burkulma yükü değerlerine, farklı fiber yönlenme açalarının etki ettiđi ve belirli bir delaminasyon çapından sonra da önemli düşüşlerin meydana geldiđi gözlenmiştir.



CONTENTS

	<u>Page</u>
Acknowledgements	I
Abstract	II
Özet	IV
Contents	VI
List of Figures	IX
List of Tables	XII
Nomenclature	XIII

Chapter One INTRODUCTION

Introduction.....	1
-------------------	---

Chapter Two LAMINATED COMPOSITES

2.1 Laminated Composites.....	4
2.2 Laminated Fibrous Composites.....	4
2.3 Basic Terminology of Laminated Fiber-Reinforced Composite Materials..	4
2.3.1 Lamina.....	4
2.3.2 Laminates.....	5
2.4 Macromechanical Behavior of an Orthotropic Lamina.....	6
2.4.1 Stress-Strain Relations for Plane Stress in an Orthotropic Material...	6
2.4.2 Stress-Strain Relations for a Lamina of Arbitrary Orientation.....	7
2.5 Buckling of Laminated Plates.....	8

Chapter Three

DELAMINATION IN LAMINATED COMPOSITES

3.1 Introduction.....	11
3.2 Causes of Delamination.....	11
3.3 Delamination Buckling.....	13

Chapter Four

EXPERIMENTAL STUDY

4.1 Preparation of Test Specimens.....	15
4.2 Determination of Mechanical Properties.....	18
4.3 Buckling Test and Determination of Critical Buckling Load.....	20

Chapter Five

NUMERICAL STUDY

5.1 Introduction.....	23
5.2 Three-Dimensional Finite Element Method.....	23
5.3 The Eight-Node Brick Element.....	25
5.4 Three-Dimensional (3D) Finite Element Model of The Laminated Composite Plates With Circular Delaminations.....	25
5.5 Buckling Analysis of The Finite Element Models With Delamination.....	27

Chapter Six

RESULTS AND DISCUSSION

Results and Discussion	31
------------------------------	----

Chapter Seven
CONCLUSION

Conclusion.....	43
References.....	45



LIST OF FIGURES

		<u>Page</u>
Figure 2.1	Two principal types of lamina.....	5
Figure 2.2	Unbounded view of laminate construction.....	6
Figure 2.3	Positive rotation of principal materials axes from x-y axes.....	8
Figure 2.4	One of basic questions of laminated plate analysis: Buckling loads=?.....	9
Figure 3	Buckling mode shapes for a delaminated composite	14
Figure 4.1	Create a delamination.....	15
Figure 4.2	Press used in manufacturing.....	16
Figure 4.3	Test specimens.....	17
Figure 4.4	Buckling test specimen.....	17
Figure 4.5	Direction of fibers on tensile specimen.....	18
Figure 4.6	Tension test specimen for determination of E_1 , E_2 and ν_{12}	19
Figure 4.7	Shear test specimen for determination of G_{12}	19
Figure 4.8	Buckling test apparatus for the two-edge clamped boundary condition.....	21
Figure 4.9	The test specimen which is loaded until buckling.....	21
Figure 4.10	Determination of the critical buckling point on the graphic.....	22
Figure 5.1	Three-dimensional problems.....	24
Figure 5.2	An eight-node brick element.....	25
Figure 5.3	Position of the single delamination.....	26
Figure 5.4	Volumes of the solid model of the laminated composite plate with single circular delamination.....	26
Figure 5.5	Interfacial areas of the volumes of the solid model.....	27
Figure 5.6	Dimensions of the layers used in the solid model.....	27
Figure 5.7	For one volume, the number of layer and fiber orientation angles at the ANSYS 6.1 program menu.....	28

	<u>Page</u>
Figure 5.8	Appearance of the solid model after meshing..... 29
Figure 5.9	Selecting the boundary conditions and applying the unit pressure... 29
Figure 6.1	Critical buckling load (P_{cr}^*) for the first test specimen without delamination and having 0 degree fiber orientation angle..... 31
Figure 6.2	Critical buckling load (P_{cr}^*) for the second test specimen without delamination and having 0 degree fiber orientation angle..... 32
Figure 6.3	Critical buckling load (P_{cr}^*) for the third test specimen without delamination and having 0 degree fiber orientation angle..... 32
Figure 6.4	Critical buckling load (P_{cr}) for the first test specimen which has 80 mm delamination and 0 degree fiber orientation angle..... 33
Figure 6.5	Critical buckling load (P_{cr}) for the second test specimen which has 80 mm delamination and 0 degree fiber orientation angle..... 33
Figure 6.6	Critical buckling load (P_{cr}) for the third test specimen which has 80 mm delamination and 0 degree fiber orientation angle..... 34
Figure 6.7	Critical buckling load (P_{cr}) for the first test specimen which has 120 mm delamination and 0 degree fiber orientation angle..... 34
Figure 6.8	Critical buckling load (P_{cr}) for the second test specimen which has 120 mm delamination and 0 degree fiber orientation angle..... 35
Figure 6.9	Critical buckling load (P_{cr}) for the third test specimen which has 120 mm delamination and 0 degree fiber orientation angle..... 35
Figure 6.10	Critical buckling load (P_{cr}) for the first test specimen which has 160 mm delamination and 0 degree fiber orientation angle..... 36
Figure 6.11	Critical buckling load (P_{cr}) for the second test specimen which has 160 mm delamination and 0 degree fiber orientation angle..... 36
Figure 6.12	Critical buckling load (P_{cr}) for the third test specimen which has 160 mm delamination and 0 degree fiber orientation angle..... 37

Page

Figure 6.13 Changing of the critical buckling loads with the delamination diameter..... 38

Figure 6.14 Changing of the critical buckling loads with the delamination diameter..... 39

Figure 6.15 Graphical comparison of the experimental and numerical results ... 40

Figure 6.16 Changing of the critical buckling loads according to the delamination diameter..... 42



LIST OF TABLES

	<u>Page</u>
Table 4.1	Prepared specimens for buckling test..... 18
Table 4.2	The mechanical properties of prepared laminated composite..... 20
Table 6.1	Critical buckling loads and average critical buckling loads for the experimental studies..... 37
Table 6.2	Critical buckling loads for the numerical studies..... 39
Table 6.3	Comparison of the experimental and numerical results..... 40
Table 6.4	Critical buckling loads for all numerical studies..... 41

NOMENCLATURE

<u>Abbreviation</u>	<u>Term</u>	<u>Unit</u>
$\sigma_1, \sigma_2, \tau_{12}$	Normal and shear stresses respectively	N/mm ²
ϵ_1, ϵ_2	Normal strains in the fiber directions	-
γ_{12}	Shearing strain	-
S_{ij}	The compliance matrix	-
E_1, E_2, E_3	Modulus of elasticity of material directions	N/mm ²
$\nu_{12}, \nu_{13}, \nu_{23}$	Poisson's ratios	-
G_{12}, G_{13}, G_{23}	Shear modulus	N/mm ²
Q_{ij}	Reduced stiffness matrix	-
θ	Fiber orientation angle	°
δ	A variation of the principal symbol from its value in the prebuckled equilibrium state	-
N	Force	N
M	Moment	Nmm
$\delta u, \delta v, \delta w$	Displacements	mm
A_{ij}	Extensional stiffness matrix	-
B_{ij}	Bending-extension coupling stiffness matrix	-
D_{ij}	Bending stiffness matrix	-
$\delta \epsilon^o, \delta \gamma^o$	The middle-surface strains	-
$\delta \kappa$	The middle-surface curvatures	-
\emptyset_1	Hole diameter	mm
\emptyset_2	Circular delamination diameter	mm
P_{cr}^*	Critical buckling load in condition without delamination	N
P_{cr}	Critical buckling load in condition with delamination	N
u	Displacement vector	-
f	Body force	N
T	Traction force	N

CHAPTER ONE

INTRODUCTION

Along with the progress of industry, the qualities of engineering of structural materials have continued to improve and their usefulness has continued to increase. Owing to their low weight and high strength, composite materials are widely used in automobile, construction and weight-sensitive aeronautical and astronautical industries. However, composite materials delaminate on occasion due to the manufacturing defects, external impact or compression loadings during their service life. The delamination problem generally results in unexpected degradation of the structure.

Various problems of delaminated composite plates under uniaxial compression have been investigated. In addition to these different solution methods have been developed according to the type of problem. The single delamination has been assumed to be near the surface and through-width has been treated as a thin film problem (1976). Chai et al. (1981) established an analytical one dimensional model for the analysis of delamination buckling of beam-plates. Vizzini and Lagace (1987) discussed the buckling of delaminated sublaminates on an elastic foundation by a Rayleigh-Ritz energy method. Wang et al. (1995) presented a continuous analysis method for determining the local buckling loads of beams and plates with single or multiple delaminations. Wang et al. (1985) dealt with delaminated random short-fibre composites by using both the Rayleigh-Ritz method and finite element buckling analysis. The problem of multiple delaminations has been considered by Kutlu and Chang (1992) by using non-linear finite element methods. Adan et al. (1994) applied one dimensional beam theory to predict the buckling load of multiple delaminations, but overlapping phenomenon was excluded.

The delaminations in the composites can be generally classified into three types of strip, circular and elliptical. Besides the strip shape of delamination has been discussed above, Chai and Babcock (1985) developed an analytical method and assessed the local buckling load of an elliptical delamination. Kassapoglou (1988) found the local buckling load by assuming a kinematically admissible power-series displacement field. Experimentally, Kassapoglou (1988) obtained the buckling load of sandwich panels made from a honeycomb core and four different facesheet lay-ups with delamination. Yeh and Tan (1994) used a non-linear finite element program based on the updated Lagrangian formulation and Newton-Raphson method in order to solve the resulting equation for the non-linear system for the buckling of the laminated plates with elliptic delamination under compressive loading. Bottega and Maewal (1983) modelled the penny-shaped delamination in circular plates as a one dimensional problem and used energy method to obtain the buckling loads.

Hwang and Mao (1999) examined the buckling behaviour of single-fiber system and interply hybrid composites with single strip delaminations by using experiments and 2D finite element method. They used carbon/epoxy and glass/epoxy composites. 0° fiber angles and different number of layers. They showed the effects of the delamination width existing on different positions in the plate, on the buckling loads and the critical delamination lengths, where the structure is not affected by the delamination. They also determined that the influence of the contact elements, used in their finite element models, on buckling loads was very small and could be neglected. Zor (2002) investigated the carbon/epoxy woven-fiber system which has been selected and in order to examine the effects of the single strip delaminations on buckling loads, linear buckling analyses of a square laminated plate have been performed for different fiber angles and simple supported boundary conditions, by using 3D finite element method. Critical delamination lengths have been determined for all cases.

In the present study, the glass/epoxy woven fibre system has been selected. In order to examine the effects of the single circular delamination in the centre of layers and different fiber orientation angles on critical buckling loads, linear buckling

analyses of a rectangular laminated composite plate have been performed for different delamination sizes and different fibre orientation angles by experimentally and numerically. In this investigation, the plates have been clamped from the two edges and loaded uniaxially from the clamped edges. The prepared laminated composite plates for the experimental studies have been manufactured from eight layers (four symmetric layers). The dimensions of these plates are 200x160x1,6 mm and they have a hole whose diameter is $\varnothing_1=40$ mm in the centre. The delamination diameters in the centre of layers of these plates have been changed as $\varnothing_2=0$ mm (without delamination), $\varnothing_2=80$ mm, $\varnothing_2=120$ mm and $\varnothing_2=160$ mm. In the experimental studies, the loading has been done only in the direction of 0 degree $[0^\circ]$ fiber orientation angle. For the numerical studies, three dimensional (3D) finite element models which have the different delamination diameter in the centre of the layers and $[0^\circ]_s$, $[15^\circ]_s$, $[30^\circ]_s$ and $[45^\circ]_s$ fiber orientation angles in order to investigate to the effect of the fiber orientation angle have been established with assistance of ANSYS 6.1 finite element analysis program. In this study, firstly, the harmony between experimentally results which were obtained from the prepared test specimens and numerical results of these test specimens has been investigated. Then, it has been seen that a good agreement between experimental results which were obtained and numerical results and in additional the numerical buckling load results of the other finite elements models which have different delamination diameters and different fiber orientation angles have been obtained.

CHAPTER TWO

LAMINATED COMPOSITES

2.1 Laminated Composites

Laminated composites consist of layers of at least two different materials that are bounded together. Lamination is used to combine the best aspects of the constituent layers in order to achieve a more useful material. The properties that can be emphasized by lamination are strength, stiffness, low weight, corrosion resistance, wear resistance, beauty or attractiveness, thermal insulation, acoustical insulation, etc.

2.2 Laminated Fibrous Composites

Laminated fibrous composites are a hybrid class of composites involving both fibrous composites and lamination techniques. A more common name is laminated fiber-reinforced composites. Here, layers of fiber-reinforced material are built up with the fiber directions of each layer typically oriented in different directions to give different strengths and stiffnesses in the various directions. Thus, the strengths and stiffnesses of the laminated fiber-reinforced composite can be tailored to the specific design requirements of the structural element being built. Examples of laminated fiber-reinforced composites include Polaris missile cases, fiberglass boat hulls, aircraft wing panels and body sections, tennis rackets, golf club shafts, etc.

2.3 Basic Terminology of Laminated Fiber-Reinforced Composite Materials

2.3.1 Lamina

A lamina is a flat (sometimes curved as in a shell) arrangement of unidirectional fibers or woven fibers in a matrix. Two typical laminas have been shown in Figure

2.1 along with their principal material axes which are parallel and perpendicular to the fiber directions. The fibers, or filaments, are the principal reinforcing or load-carrying agent. They are typically strong and stiff. The matrix can be organic, ceramic or metallic. The function of the matrix is to support and protect the fibers and to provide a means of distributing load among and transmitting load between the fibers. Fibers generally exhibit linear elastic behavior, although reinforcing steel bars in concrete are more nearly elastic perfectly plastic. Aluminum and some composites exhibit elastic-plastic behavior which is really non-linear elastic behavior if there is no unloading.

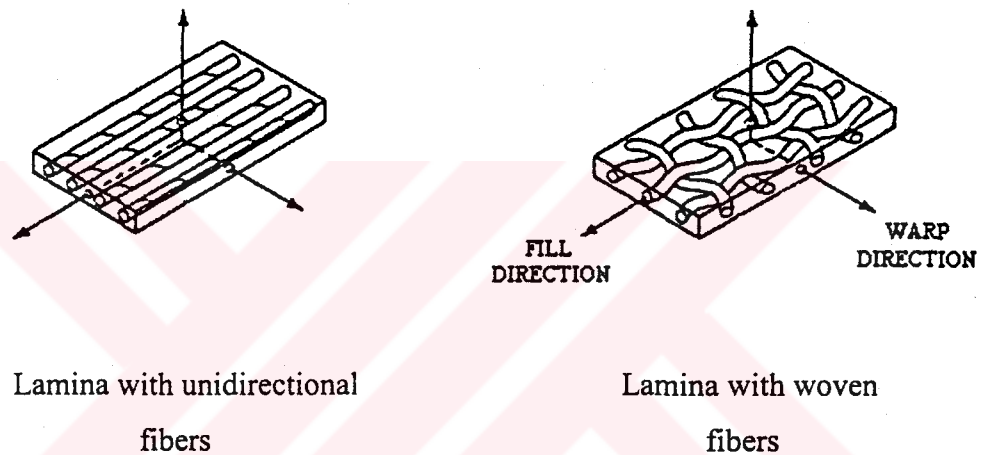


Figure 2.1 Two principal types of lamina.

2.3.2 Laminates

A laminate is a stack of lamina with various orientations of principal material directions in the lamina as in Figure 2.2. Note that the fiber orientation of the layers in Figure 2.2 is not symmetric about the middle surface of the laminate. The layers of a laminate are usually bound together by the same matrix material that is used in the lamina. Laminates can be composed of plates of different materials or layers of fiber-reinforced lamina. A laminated circular cylindrical shell can be constructed by winding resin-coated fibers on a mandrel first with one orientation to the shell axis, then another, and so on until the desired thickness is built up.

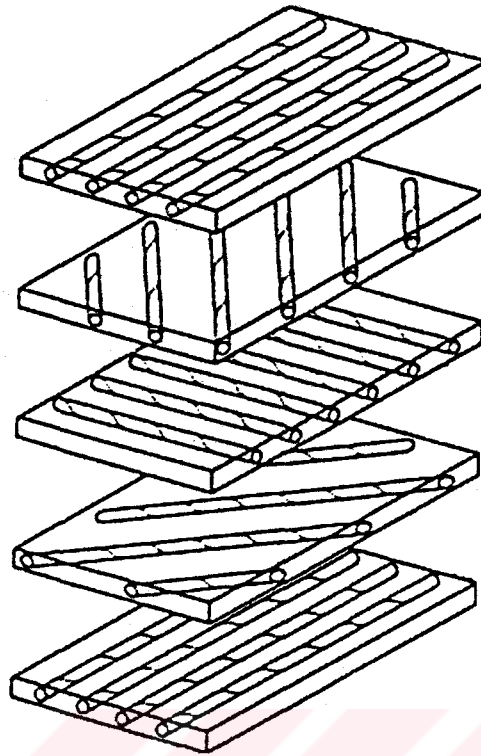


Figure 2.2 Unbounded view of laminate construction.

2.4 Macromechanical Behavior of an Orthotropic Lamina

2.4.1 Stress-Strain Relations for Plane Stress in an Orthotropic Material

Two dimensional strain-stress relations in an orthotropic material can be written as:

$$\begin{Bmatrix} \varepsilon_1 \\ \varepsilon_2 \\ \gamma_{12} \end{Bmatrix} = \begin{bmatrix} S_{11} & S_{12} & 0 \\ S_{12} & S_{22} & 0 \\ 0 & 0 & S_{66} \end{bmatrix} \begin{Bmatrix} \sigma_1 \\ \sigma_2 \\ \tau_{12} \end{Bmatrix} \quad (2.1)$$

where

$$S_{11} = \frac{1}{E_1}, \quad S_{12} = -\frac{\nu_{12}}{E_1} = -\frac{\nu_{21}}{E_2}, \quad S_{22} = \frac{1}{E_2}, \quad S_{66} = \frac{1}{G_{12}} \quad (2.2)$$

The strain-stress relations in Equation 2.1 can be inverted to obtain the stress-strain relations:

$$\begin{Bmatrix} \sigma_1 \\ \sigma_2 \\ \tau_{12} \end{Bmatrix} = \begin{bmatrix} Q_{11} & Q_{12} & 0 \\ Q_{12} & Q_{22} & 0 \\ 0 & 0 & Q_{66} \end{bmatrix} \begin{Bmatrix} \varepsilon_1 \\ \varepsilon_2 \\ \gamma_{12} \end{Bmatrix} \quad (2.3)$$

or, in terms of the engineering constant,

$$Q_{11} = \frac{E_1}{1 - \nu_{12}\nu_{21}}, Q_{12} = \frac{\nu_{12}E_2}{1 - \nu_{12}\nu_{21}} = \frac{\nu_{21}E_1}{1 - \nu_{12}\nu_{21}}, Q_{22} = \frac{E_2}{1 - \nu_{12}\nu_{21}}, Q_{66} = G_{12} \quad (2.4)$$

Note that there are four independent material properties, E_1 , E_2 , G_{12} , ν_{12} . (Jones, 1999)

2.4.2 Stress-Strain Relations for a Lamina of Arbitrary Orientation

In Section 2.4.1, the stresses and strains have been defined in the principal material coordinates for an orthotropic material. However, the principal directions of orthotropy often do not coincide with coordinate directions that are geometrically natural to the solution of the problem. For this reason a method of transforming stress-strain relations from one coordinate system to another is needed.

The principal material axes and θ , is the angle from the x-axis to 1- axis, have been shown in Figure 2.3.

The stress-strain relations in x-y coordinates are

$$\begin{Bmatrix} \sigma_x \\ \sigma_y \\ \tau_{xy} \end{Bmatrix} = \begin{bmatrix} \bar{Q}_{11} & \bar{Q}_{12} & \bar{Q}_{16} \\ \bar{Q}_{12} & \bar{Q}_{22} & \bar{Q}_{26} \\ \bar{Q}_{16} & \bar{Q}_{26} & \bar{Q}_{66} \end{bmatrix} \begin{Bmatrix} \varepsilon_x \\ \varepsilon_y \\ \gamma_{xy} \end{Bmatrix} \quad (2.5)$$

in which

$$\begin{aligned}
\bar{Q}_{11} &= Q_{11} \cos^4 \theta + 2(Q_{12} + 2Q_{66}) \sin^2 \theta \cos^2 \theta + Q_{22} \sin^4 \theta \\
\bar{Q}_{12} &= (Q_{11} + Q_{22} - 4Q_{66}) \sin^2 \theta \cos^2 \theta + Q_{12}(\sin^4 \theta + \cos^4 \theta) \\
\bar{Q}_{22} &= Q_{11} \sin^4 \theta + 2(Q_{12} + 2Q_{66}) \sin^2 \theta \cos^2 \theta + Q_{22} \cos^4 \theta \\
\bar{Q}_{16} &= (Q_{11} - Q_{12} - 2Q_{66}) \sin \theta \cos^3 \theta + (Q_{12} - Q_{22} + 2Q_{66}) \sin^3 \theta \cos \theta \\
\bar{Q}_{26} &= (Q_{11} - Q_{12} - 2Q_{66}) \sin^3 \theta \cos \theta + (Q_{12} - Q_{22} + 2Q_{66}) \sin \theta \cos^3 \theta \\
\bar{Q}_{66} &= (Q_{11} + Q_{22} - 2Q_{12} - 2Q_{66}) \sin^2 \theta \cos^2 \theta + Q_{66}(\sin^4 \theta + \cos^4 \theta)
\end{aligned} \tag{2.6}$$

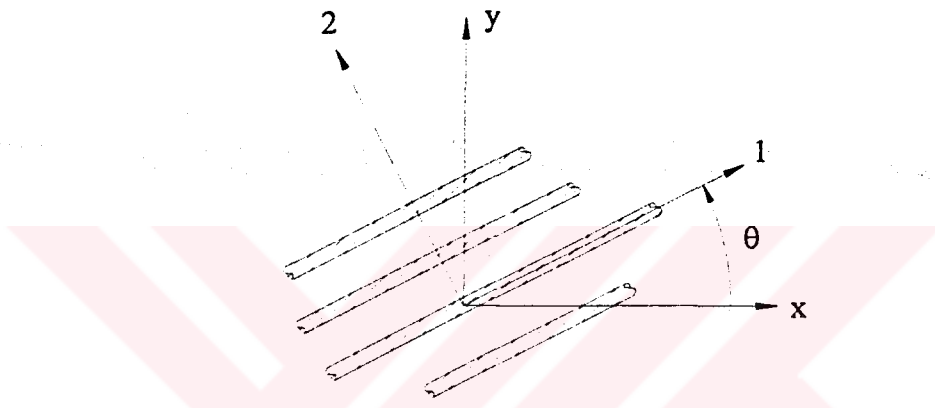


Figure 2.3 Positive rotation of principal materials axes from x-y axes.

where the bar over the \bar{Q}_{ij} matrix denotes that we are dealing with the transformed reduced stiffnesses instead of the reduced stiffnesses, Q_{ij} . (Jones, 1999)

2.5. Buckling of Laminated Plates

A plate buckles when the in-plane compressive load gets so large that the originally flat equilibrium state is no longer stable, and the plate deflects into a nonflat configuration. The load at which the departure from the flat state takes place is called the buckling load. The flat equilibrium state has only in-plane forces and undergoes only extension, compression and shear. Thus, the flat equilibrium state is often called the membrane prebuckled state and consists of only in-plane deformations.

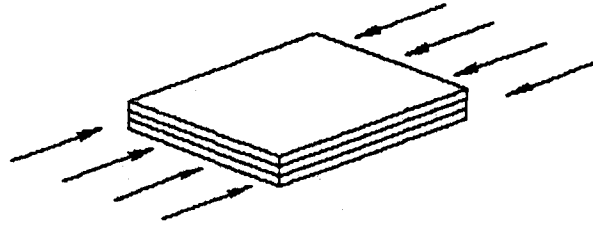


Figure 2.4 One of basic questions of laminated plate analysis: Buckling loads=?.

Analysis of plates buckling under in-plane loading involves solution of an eigenvalue problem as opposed to the boundary value problem of equilibrium analysis. The distinctions between boundary value problems and eigenvalue problems are too involved to treat here. Instead, the buckling differential equations governing the buckling behavior from a membrane prebuckled state are

$$\delta N_{x,x} + \delta N_{xy,y} = 0 \quad (2.7)$$

$$\delta N_{xy,x} + \delta N_{y,y} = 0 \quad (2.8)$$

$$\delta M_{x,xx} + 2\delta M_{xy,xy} + \delta M_{y,yy} + \overline{N}_x \delta w_{,xx} + 2\overline{N}_{xy} \delta w_{,xy} + \overline{N}_y \delta w_{,yy} = 0 \quad (2.9)$$

where δ denotes a variation of the principle symbol from its value in the prebuckled equilibrium state. Thus, the terms $\delta N_x, \dots, \delta M_x, \dots$ are variations of forces and moments, respectively, from their values in a membrane prebuckling equilibrium state. The term δw is variations in displacement from the same flat prebuckled state. Note that if the prebuckling state is a membrane, then $\delta w = w$ because there is no prebuckling out-of-plane displacement. Also note that the applied in-plane loads \overline{N}_x , \overline{N}_y and \overline{N}_{xy} enter the mathematical formulation of the eigenvalue problem as coefficients of the curvatures rather than as 'loads' on the right-hand side of the equilibrium equation.

The variations in force and moment resultants are

$$\begin{bmatrix} \delta N_x \\ \delta N_y \\ \delta N_{xy} \end{bmatrix} = \begin{bmatrix} A_{11} & A_{12} & A_{16} \\ A_{21} & A_{22} & A_{26} \\ A_{16} & A_{26} & A_{66} \end{bmatrix} \begin{bmatrix} \delta \varepsilon_x^\circ \\ \delta \varepsilon_y^\circ \\ \delta \gamma_{xy}^\circ \end{bmatrix} + \begin{bmatrix} B_{11} & B_{12} & B_{16} \\ B_{21} & B_{22} & B_{26} \\ B_{16} & B_{26} & B_{66} \end{bmatrix} \begin{bmatrix} \delta \kappa_x \\ \delta \kappa_y \\ \delta \kappa_{xy} \end{bmatrix} \quad (2.10)$$

$$\begin{bmatrix} \delta M_x \\ \delta M_y \\ \delta M_{xy} \end{bmatrix} = \begin{bmatrix} B_{11} & B_{12} & B_{16} \\ B_{21} & B_{22} & B_{26} \\ B_{16} & B_{26} & B_{66} \end{bmatrix} \begin{bmatrix} \delta \varepsilon_x^\circ \\ \delta \varepsilon_y^\circ \\ \delta \gamma_{xy}^\circ \end{bmatrix} + \begin{bmatrix} D_{11} & D_{12} & D_{16} \\ D_{21} & D_{22} & D_{26} \\ D_{16} & D_{26} & D_{66} \end{bmatrix} \begin{bmatrix} \delta \kappa_x \\ \delta \kappa_y \\ \delta \kappa_{xy} \end{bmatrix} \quad (2.11)$$

where the variations in in-plane strains and changes in curvature are related to the variations in displacements by

$$\delta \varepsilon_x^\circ = \delta u_{,x} \quad \delta \varepsilon_y^\circ = \delta v_{,y} \quad \delta \gamma_{xy}^\circ = \delta u_{,y} + \delta v_{,x} \quad (2.12)$$

$$\delta \kappa_x = -\delta w_{,xx} \quad \delta \kappa_y = -\delta w_{,yy} \quad \delta \kappa_{xy} = -2\delta w_{,xy} \quad (2.13)$$

The buckling differential equations can be expressed in terms of the variations in displacements by substituting the variations in in-plane strains and curvatures, Equations (2.12) and (2.13), in the variations in force and moment resultants, Equations (2.10) and (2.11), and subsequently in the buckling differential equations in terms of the variations of forces, moments and displacements during buckling, i.e., Equations (2.7) to (2.9). However, some special laminates exhibit no bending-extension coupling; hence, their buckling loads are obtained by solution of only Equation (2.8) or its variation of deflections equivalent. (Jones, 1999)

CHAPTER THREE

DELAMINATION IN LAMINATED COMPOSITES

3.1 Introduction

Laminated composite materials, especially in the form of fiber reinforced plastics, are being utilized increasingly in the design of various structural applications. This is mostly due to the fact that these materials enjoy strength to weight ratio advantage over the ordinary engineering materials. In spite of their definite advantages, they suffer from a major problem, namely their weak strength in the through the thickness direction of laminate because of low cohesive strength between the layers.

The defect could be even worse if the composite contains delamination. Delamination in composite may develop during manufacturing because of the imperfections and/or faulty procedures, or during service, by impact of an external object. This can significantly reduce the compressive strength and stiffness of the laminate and thereby, lowering the buckling load of the laminate when subjected to a compressive load, causing growth of such delamination regions.

3.2 Causes of Delamination

Lamination of composite structures is one of the most common manufacturing techniques used in the construction of composite components. As the applications of composites expand, the use of laminated components in primary structures is becoming more prevalent. One of the limiting factors of laminated structures is a failure mode known as delamination. Delamination is the most common reason for

laminated composite component failure and is the separation of individual layers of the laminated structure.

Delamination in laminated composites may originate from a number of sources. These sources can be broadly grouped as:

a. Manufacturing Defects: Improper manufacturing techniques, impurities, or manufacturing errors can result in a poor bond between successive layers of laminates.

b. Impact Damage: Impact damage to composites is one of the primary design limitations of composite structures. Impact damage can be classed as either: High Velocity Impact (HVI) or Low Velocity Impact (LVI). Some text also refers to Medium Velocity Impact but this class has been included in HVI for the purpose of discussion.

b.1. High Velocity Impact (HVI): HVI will cause significant surface damage and should therefore, be easily recognized. Through penetration may result. The area of the exit damage has been shown to increase linearly with component thickness. In addition to the surface damage, there may also be significant delamination around the impact site. NDI procedures will typically be used to determine the extent of the damage.

b.2. Low Velocity Impact (LVI): Internal delaminations can result from LVI. In this class of damage, it is possible that there will be no significant sign of surface damage. The delaminations and subsequent loss of structural integrity may remain undetected. For this reason the composite allowable design strain is normally limited to approximately 0.4% of the ultimate design strain.

c. Three Dimensional Interlaminar Stresses: Composites exhibit very high directional strength properties. This advantage enables designers to purposely align plies in the direction of load; however, where the application of load is out of plane or where the load is transferred to adjacent plies with varying ply direction,

interlaminar stress may cause delamination. Composites structures rely on the strength of the fiber to support load, typically the matrix carries very little of the applied load. If stress is applied normal (in the z direction) to the ply direction, then the matrix must support the full load and delamination is likely. Similarly, the matrix alone may be required to support shear stresses in the xz and yz planes.

d. Compressive Loading: Interlaminar stresses can also be introduced by compressive loading. Buckling of the plies and subsequently delamination may then result. Composite laminates have shown good resistance to cyclic tensile stresses but the fatigue life of composites is adversely affected by excursions into compressive loading. Once initiated, delamination crack growth under fatigue conditions is relatively fast.

3.3 Delamination Buckling

Delamination buckling may occur in different types of model shapes. As shown in Figure 3, at the critical load level, a compressed beam having a single delamination may respond in three possible modes of instability. Delamination length and its position through the thickness are the two important parameters controlling the shape of these modes. If the entire beam buckles before any other mode of deflection could take place, the response is referred to as the “global” buckling mode. This usually occurs in relatively short and thick delaminated beams. In a global buckling mode, if the buckling shape is symmetric with respect to the midspan of the beam, it is identified as the “global symmetric” mode (Figure 3.a). On the other hand, if the global buckling mode tends to deform into a kinked shape, the buckling shape is called the “global antisymmetric” mode (Figure 3.b). When the delamination is thin, the first region that buckles is the delaminated region. Such a buckling is declared as the “local” buckling mode (Figure 3.c). Finally, in an axially compressed delaminated beam, if both the global and local buckling take place at the same time, then the response is referred to as the “mixed” buckling mode (Figure 3.d). The situations for multiply delaminated beams are quite similar to the ones discussed for single delamination.

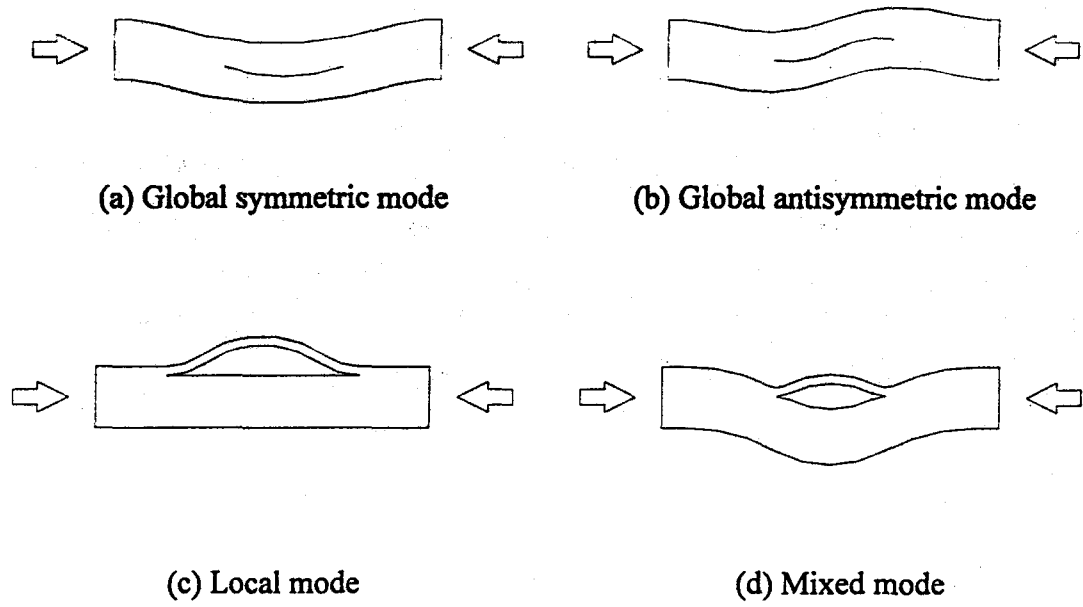


Figure 3 Buckling mode shapes for a delaminated composite.

In the experimental studies, it has been seen that test specimens were buckled according to global symmetric mode. (Figure 4.9)

CHAPTER FOUR

EXPERIMENTAL STUDY

4.1 Preparation of Test Specimens

The specimens which were used in this investigation have been fabricated in Izoreel Composite Isolate Materials Company from glass-epoxy prepreg layers which called EP GC 203 in Izoreel Composites Catalogue. In this prepreg layers, woven glass fiber as fiber and epoxy as resin have been used. Thickness of these glass-epoxy prepreg layers which are imported from abroad are 0.2 mm.

During the fabrication process, eight layers from this prepreg layers have been used to prepare the specimens. Teflon film which has 13 μm thickness has been used in order to create delamination between layers.

Firstly, four laminates have been located one on the top of the other. Then, teflon film which has different diameters has been placed between fourth and fifth layers to create different delamination sizes. Finally, the other four layers have been located successively (Figure 4.1).

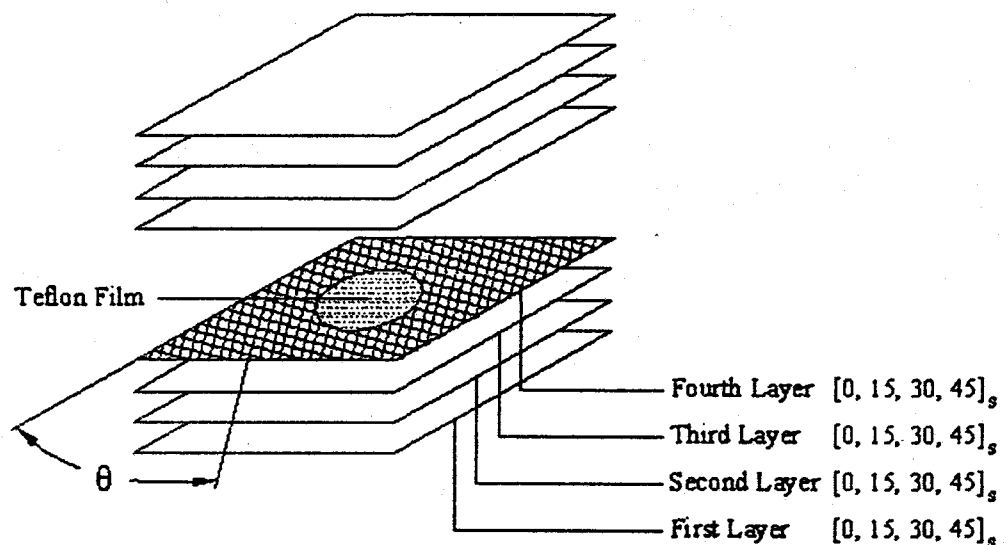


Figure 4.1 Create a delamination.

Angles of layers have been shown in Figure 4.1 for the test specimens which have different fiber orientation angles. Enumerating of layers are $[0, 0, 0, 0 \parallel 0, 0, 0, 0]$ for the $[0^\circ_4]_s$ laminated composites, $[15, 15, 15, 15 \parallel 15, 15, 15, 15]$ for the $[15^\circ_4]_s$ laminated composites, $[30, 30, 30, 30 \parallel 30, 30, 30, 30]$ for the $[30^\circ_4]_s$ laminated composites, $[45, 45, 45, 45 \parallel 45, 45, 45, 45]$ for the $[45^\circ_4]_s$ laminated composites. Where, the sign (\parallel) gives the position of the delamination in the laminated composites.

Then, prepared layers have been pressed at 100°C , under 12 MPa pressure, in the course of 2 hours in the hydraulic press (Figure 4.2).

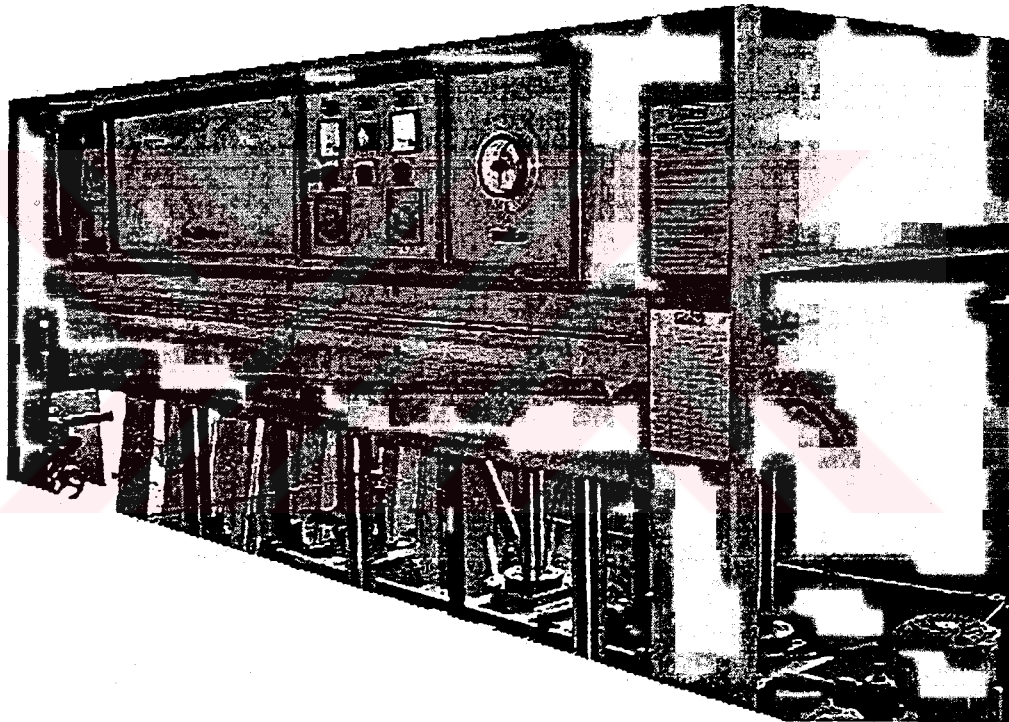


Figure 4.2 Press used in manufacturing.

Thus, laminated composites with delamination have been obtained (Figure 4.3). Thickness of the test specimens where coming off from the press is 1.6 mm. For the experimental studies, test specimens which have only 0 degree $[0^\circ]$ fiber orientation angles have been produced.

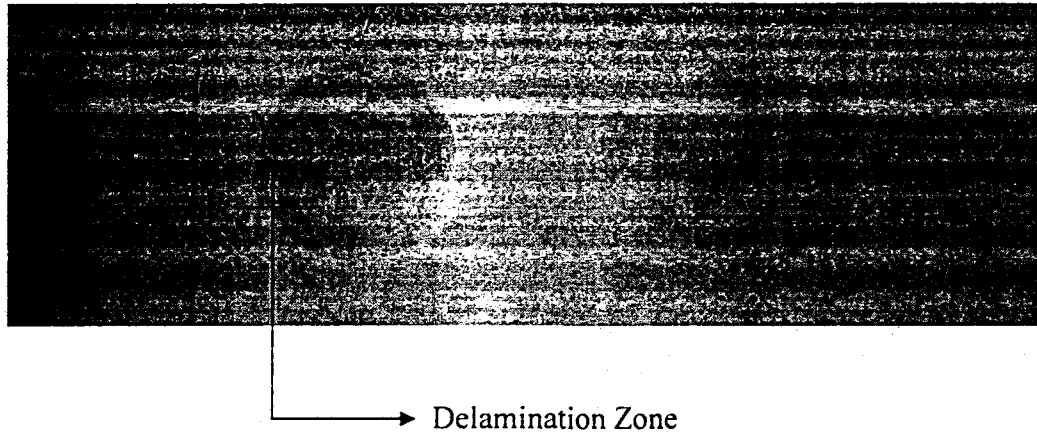


Figure 4.3 Test specimens.

Prepared test specimens have been cut in the size of 200x200 mm and cut out a hole which has 40 mm diameter in the centre of plate to be used in the tests (Figure 4.4). However, for the buckling tests, the real height is 160 mm. Because of the clamped boundary condition, it has been left a margin 20 mm from the top and bottom edges. Thus, dimensions of the buckling test specimen are 200x160x1.6 mm.

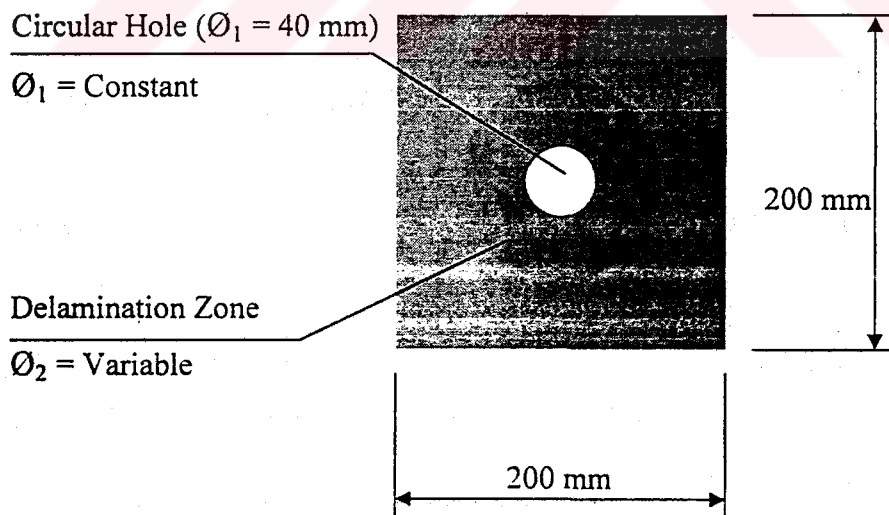


Figure 4.4 Buckling test specimen.

Diameters and fiber orientation angles of the test specimens for the buckling tests have been given in Table 4.1.

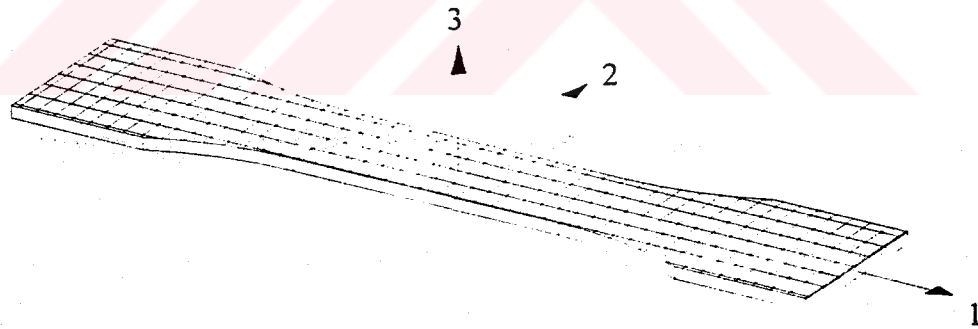
Table 4.1 Prepared specimens for buckling test.

Hole Diameter (mm)	Delamination Diameter (mm)	Fiber Orientation Angle (°)
$\varnothing_1=40$	$\varnothing_2=0$	0
$\varnothing_1=40$	$\varnothing_2=80$	0
$\varnothing_1=40$	$\varnothing_2=120$	0
$\varnothing_1=40$	$\varnothing_2=160$	0

Delamination diameter $\varnothing_2=0$ has been called test specimen without delamination. Also test specimen without delamination is called as test specimen only with hole.

4.2 Determination of Mechanical Properties

To obtain E_1 , E_2 , ν_{12} , a rectangular specimen whose fiber directions coincides with the loading direction on Figure 4.5 has been taken and two strain gauges perpendicular to each other have been stuck on Figure 4.6. All of them were in the fiber direction.

**Figure 4.5** Direction of fibers on tensile specimen.

The specimen has been loaded step by step to rupture by a Shimadzu 50 kNG Tensile Machine. For all steps, ε_1 and ε_2 have been measured by an indicator. By using these strains E_1 , E_2 and ν_{12} have been obtained. Because of the prepared laminated composite is woven, E_2 is equal to E_1 .

$$E_x = \frac{P/A}{\epsilon_x}$$

$$G_{12} = \frac{1}{\frac{4}{E_x} - \frac{1}{E_1} - \frac{1}{E_2} + \frac{2\nu_{12}}{E_1}} \quad (\text{Jones, 1999}) \quad (4.2)$$

Since, the strain gauge couldn't be stuck to direction 3, G_{13} and G_{23} haven't been found by experiment. Therefore, it has been assumed that, G_{13} and G_{23} are equal to G_{12} .

The mechanical properties which were obtained from the experimental study have been given in Table 4.2.

Table 4.2 The mechanical properties of prepared laminated composite.

$E_1=E_2$ (MPa)	E_3 (MPa)	ν_{12} (MPa)	$\nu_{13}=\nu_{23}$ (MPa)	$G_{12}=G_{13}=G_{23}$ (MPa)
27000	16200	0.15	0.09	7540

4.3 Buckling Test and Determination of Critical Buckling Load

The buckling tests have been done in compression mode on the Shimadzu 50 kNG Test Machine. In the course of experiments, test apparatus which has two clamped edges and other two edges free has been used (Figure 4.8).

For each delamination diameter, three identical specimens have been tested. During the testing, all specimens have been loaded until the buckling (Figure 4.9) and the results have been obtained in the case of text file on the test machine. Then, the text files have been opened by Excel and the graphics of the experimental results have been drawn.

For determination of critical buckling load, the point where left from the straight line has been determined on the graphics of the experimental results and the value on

the y axis of this point has been called as the critical buckling load (Figure 4.10).

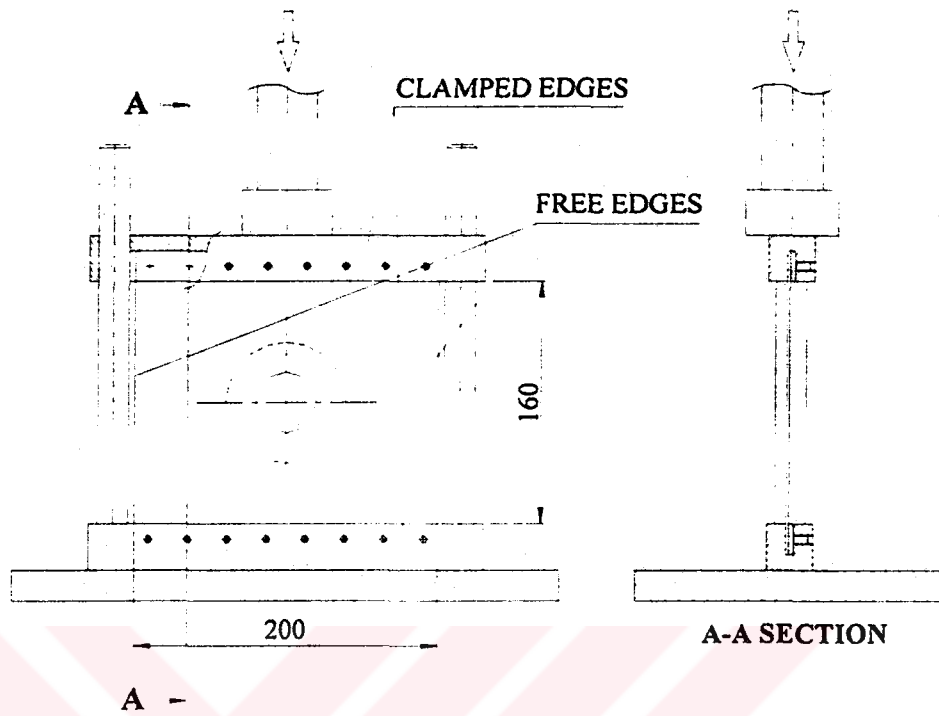


Figure 4.8 Buckling test apparatus for the two-edge clamped boundary condition.
(where all dimensions are mm)

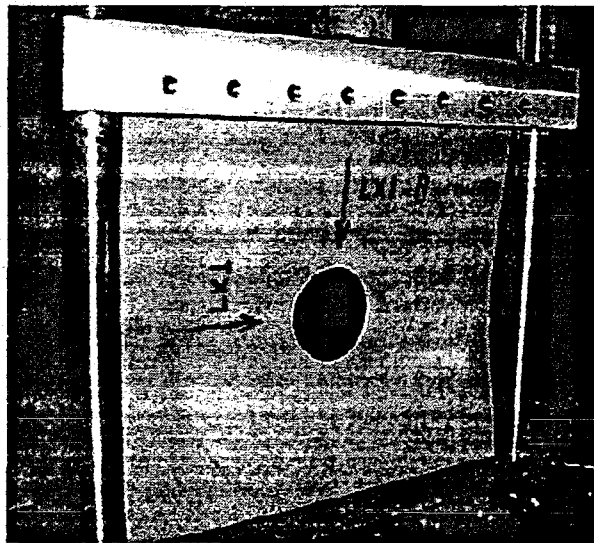


Figure 4.9 The test specimen which is loaded until buckling.

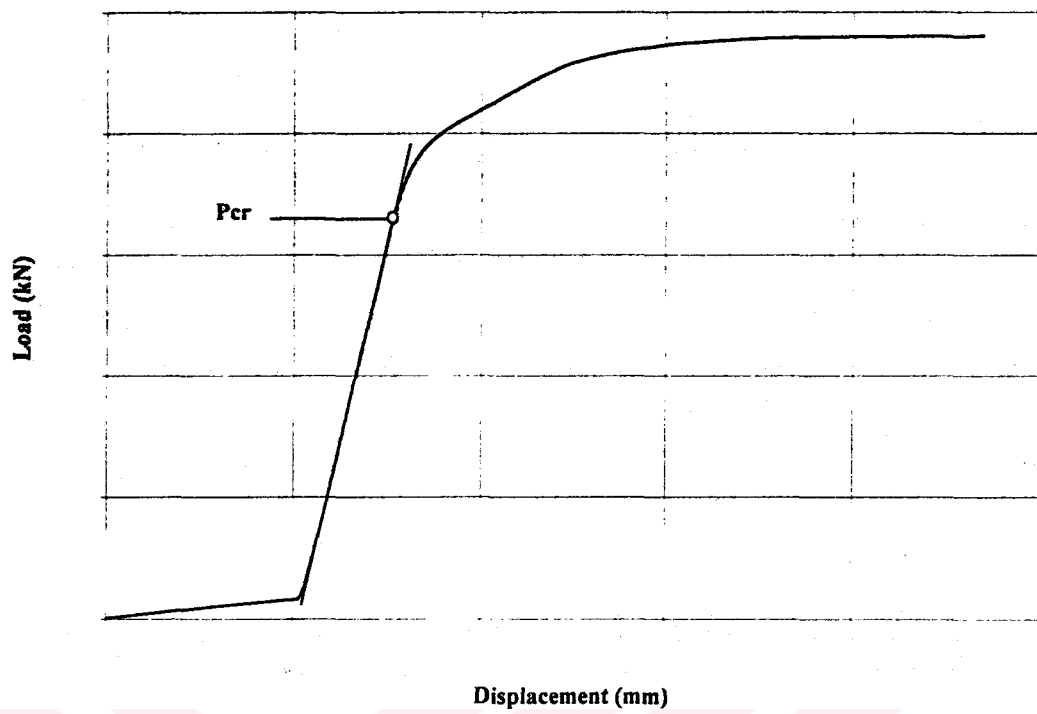


Figure 4.10 Determination of the critical buckling point on the graphic.

CHAPTER FIVE

NUMERICAL STUDY

5.1 Introduction

The finite element method has become a powerful tool in the numerical solution of a wide range of engineering problems. Application range is from deformation and stress analysis of automotive, aircraft, building, and bridge structures to field analysis of heat flux, fluid flow, magnetic flux, seepage, and other flow problems. In this method of analysis, a complex region defining a continuum is discretized into simple geometric shapes called finite elements. The material properties and the governing relationships are considered over these elements and expressed in terms of unknown values of the element. An assembly process, duly considering the loading and constraints, results in a set of equations. Solution of these equations gives the approximate behavior of the continuum (Chandrupatla, 1991).

5.2 Three-Dimensional Finite Element Method

In the three-dimensional finite element formulation, the displacements, traction components and distributed body force values are the functions of the position indicated by (x, y, z) . The displacement vector \mathbf{u} is given as

$$\mathbf{u} = [u, v, w]^T \quad (5.1)$$

where u , v and w are the x , y and w components of \mathbf{u} , respectively. The stress and strains are given by

$$\boldsymbol{\sigma} = [\sigma_x, \sigma_y, \sigma_z, \tau_{xy}, \tau_{xz}, \tau_{yz}]^T \quad (5.2)$$

$$\boldsymbol{\varepsilon} = [\varepsilon_x, \varepsilon_y, \varepsilon_z, \gamma_{xy}, \gamma_{xz}, \gamma_{yz}]^T$$

From Figure 5.1, representing the three-dimensional problem in a general setting, the body force, traction vector, and elemental volume are given by

$$\mathbf{f} = [f_x, f_y, f_z]^T, \quad \mathbf{T} = [T_x, T_y, T_z]^T \quad \text{and} \quad dV = t dA \quad (5.3)$$

where t is the thickness along the z direction. The body force \mathbf{f} has unit of force per unit volume, while the traction force \mathbf{T} has unit of force per unit area.

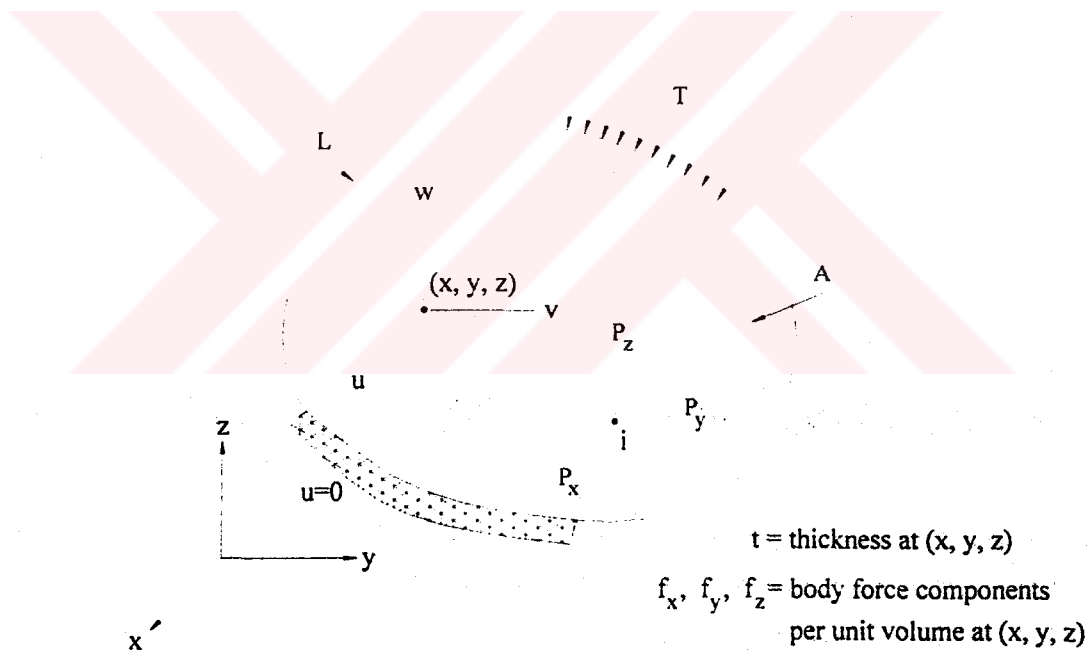


Figure 5.1 Three-dimensional problems.

5.3 The Eight-Node Brick Element

The eight-node brick element is a simple three-dimensional element used in the analysis of solid mechanics problems. Each of the eight nodes of this element has three translational degrees of freedom in the nodal x , y and z directions. A typical eight-node brick element is shown in Figure 5.2 (Moaveni, 1999).

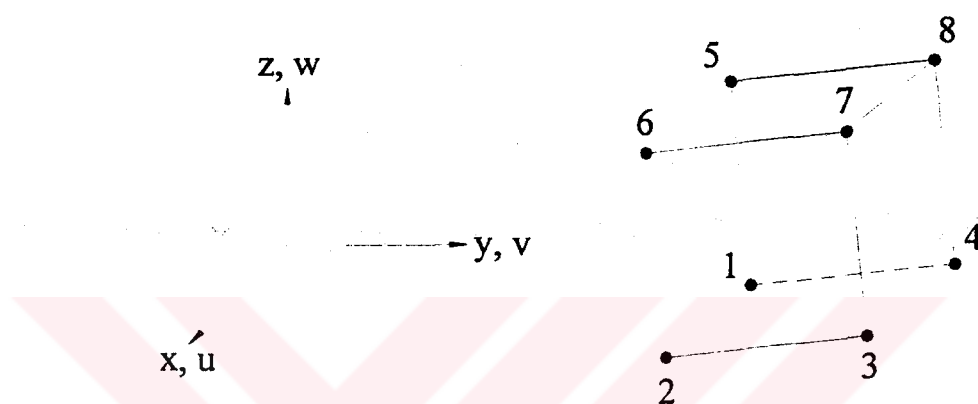


Figure 5.2 An eight-node brick element.

5.4 Three-Dimensional (3D) Finite Element Model of The Laminated Composite Plates with Circular Delaminations

In the design of 3D finite element model of the laminated composite plates having different single circular delamination (Figure 5.3), the solid model contains thirty two volumes. Sixteen volumes of these volumes are at the top region and other sixteen volumes are at the bottom region (Figure 5.4). But, some areas in the interfaces of this top and bottom volumes are not the same although these areas have the same dimensions and coordinates (Figure 5.5).

While, A9, A11, A13, A15, A17, A19, A21, A23 areas belong to the upper V9, V11, V13, V15, V17, V19, V21, V23 volumes; A10, A12, A14, A16, A18, A20, A22, A24 areas which have the same dimensions and coordinates with A9, A11,

A13, A15, A17, A19, A21, A23 areas respectively, belong to the bottom V10, V12, V14, V16, V18, V20, V22, V24 volumes. The lateral areas, A1, A2, A3, A4, A5, A6, A7, A8, are the common areas of the top and bottom lateral volumes. When the volumes are meshed, double nodes occur at the same coordinates of the interfacial areas without lateral areas. Thus, the solid modeling of the single circular delamination can be modeled.

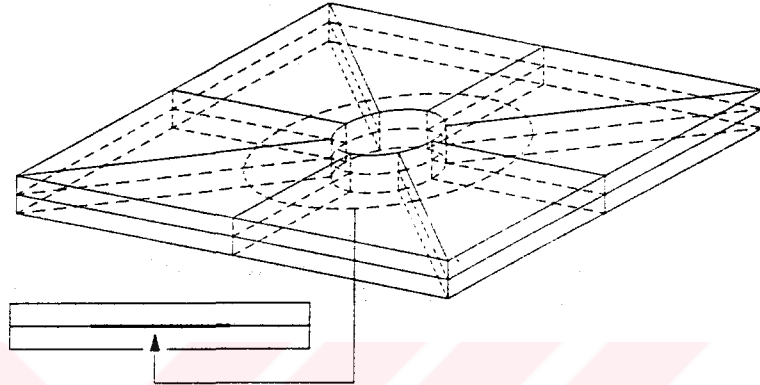


Figure 5.3 Position of the single delamination.

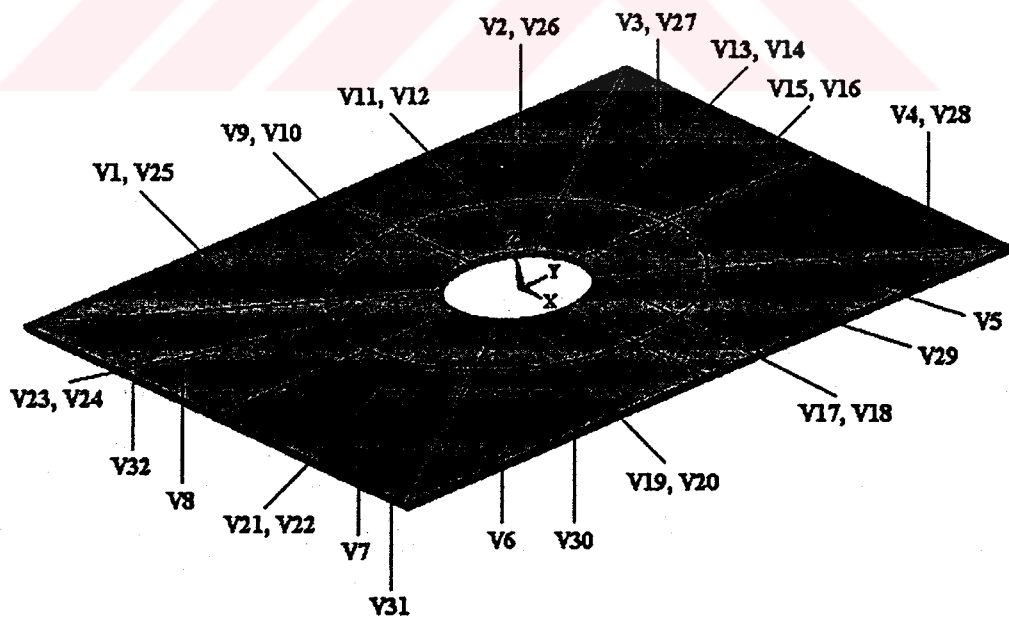


Figure 5.4 Volumes of the solid model of the laminated composite plate with single circular delamination.

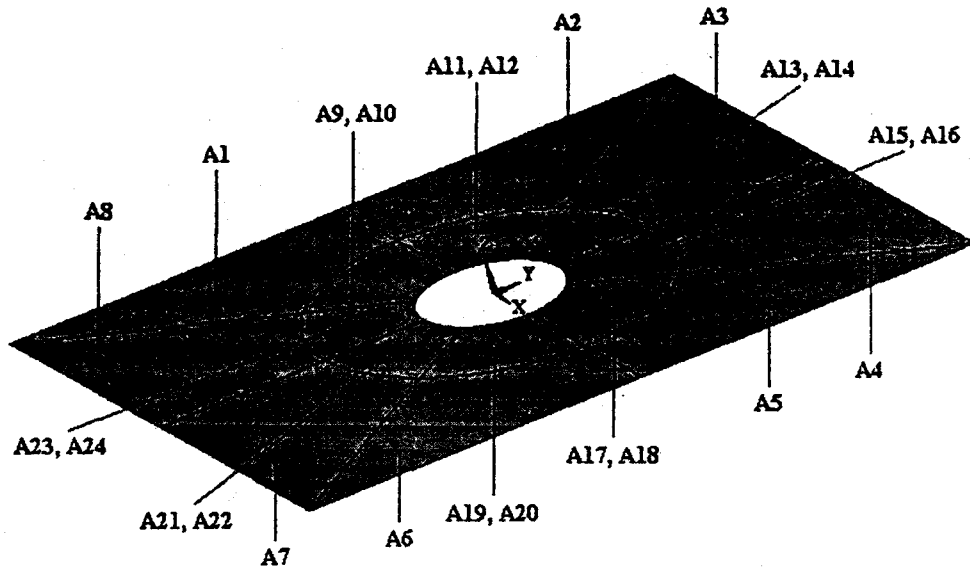


Figure 5.5 Interfacial areas of the volumes of the solid model.

5.5 Buckling Analysis of The Finite Element Models with Delamination

Firstly, the solid models of the laminated composite plate with two volumes and eight layers and different delamination diameters (ϕ_2) have been prepared by using ANSYS 6.1. Each of the layers has 200x160x 0.2 mm dimensions (Figure 5.6).

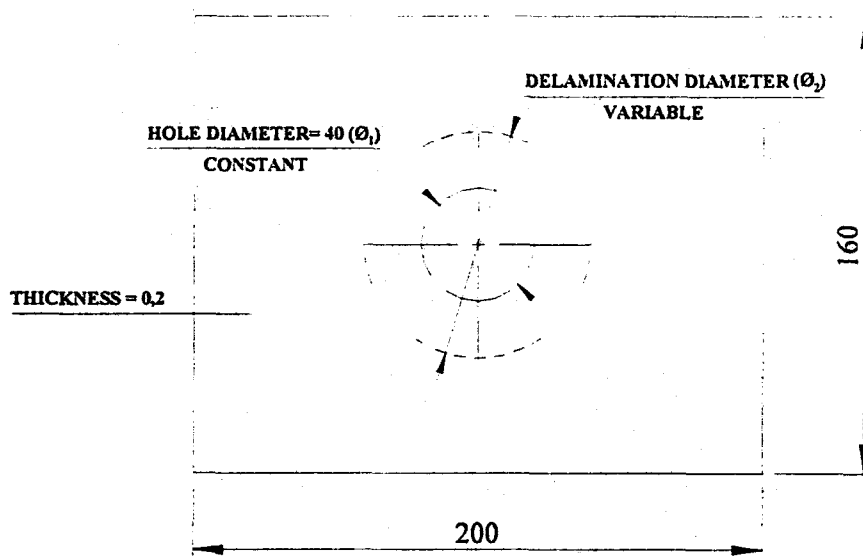


Figure 5.6 Dimensions of the layers used in the solid model.

The delamination region has been existed between two volumes (between fourth and fifth layers). The diameters of the circular delamination (\varnothing_2) are 0 (without delamination), 45, 50, 55, 60, 65, 70, 80, 100, 120, 140, 160 mm respectively. In this case, 11 models with different delamination diameters have been obtained. However, each model has four different fiber orientation ($[0^{\circ}_4]_s$, $[15^{\circ}_4]_s$, $[30^{\circ}_4]_s$, $[45^{\circ}_4]_s$). Thus, 44 models have been totally obtained.

After the modeling of the laminated composite plate, element type, number of layers, thickness of layers and fiber orientation angles have been determined. Each volume has been constituted from four layers which have 0.2 mm thickness. The element type, SOLID46 which is called eight-node brick element has been assigned. Then, fiber orientation angles (Figure 5.7) and material properties have been assigned.

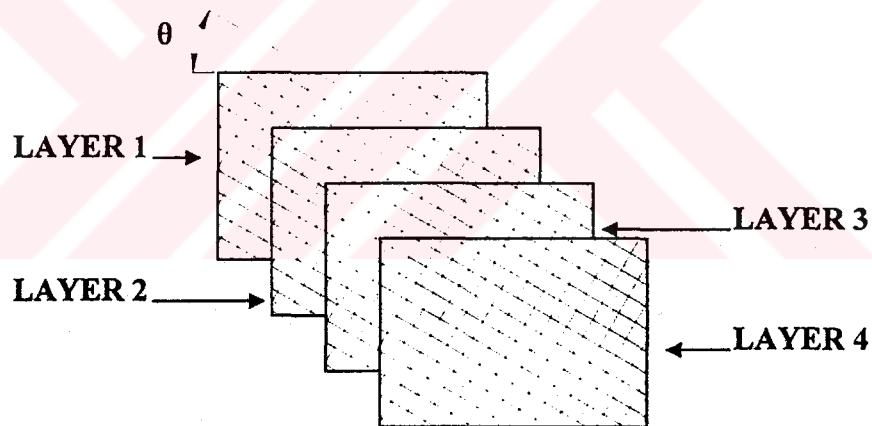


Figure 5.7 For one volume, the number of layer and fiber orientation angles at the ANSYS 6.1 program menu.

After all of the properties were selected, the solid model has been meshed (Figure 5.8).

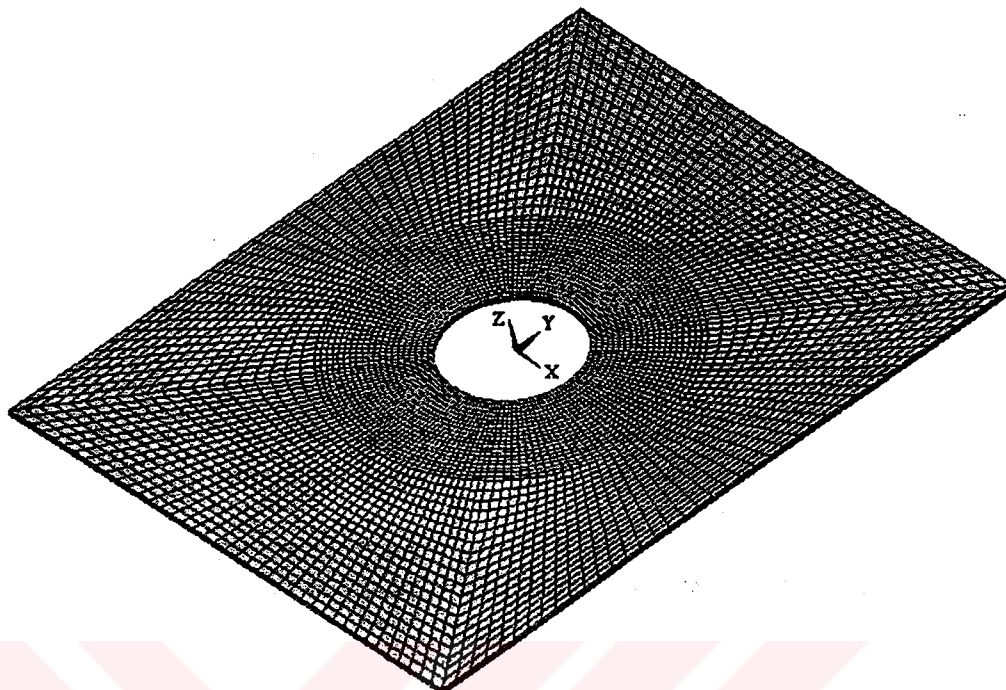


Figure 5.8 Appearance of the solid model after meshing.

Then, boundary conditions have been selected and unit pressure has been applied to the right edge (Figure 5.9).

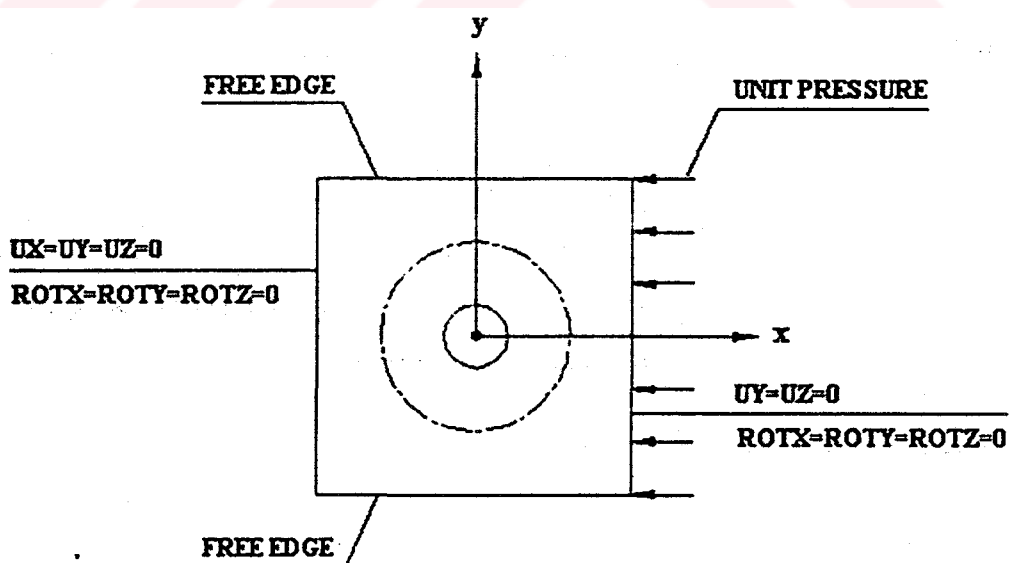


Figure 5.9 Selecting the boundary conditions and applying the unit pressure.

The element types, boundary conditions and loads of these models have been taken as the same as the model without delamination.

Finally, the problem has been solved by the ANSYS 6.1 finite element analysis program and for the different delamination sizes and different fiber orientation angles. Thus, the critical buckling loads have been obtained numerically.



CHAPTER SIX

RESULTS AND DISCUSSION

In the experimental studies, the critical buckling loads have been obtained for the test specimens which have $\varnothing_2=0$ mm (without delamination), $\varnothing_2=80$ mm, $\varnothing_2=120$ mm and $\varnothing_2=160$ mm delamination diameters and 0 degree $[0^\circ]$ fiber orientation angle. These critical buckling loads have been given in the graphics between Figure 6.1 and Figure 6.12 and in Table 6.1 respectively.

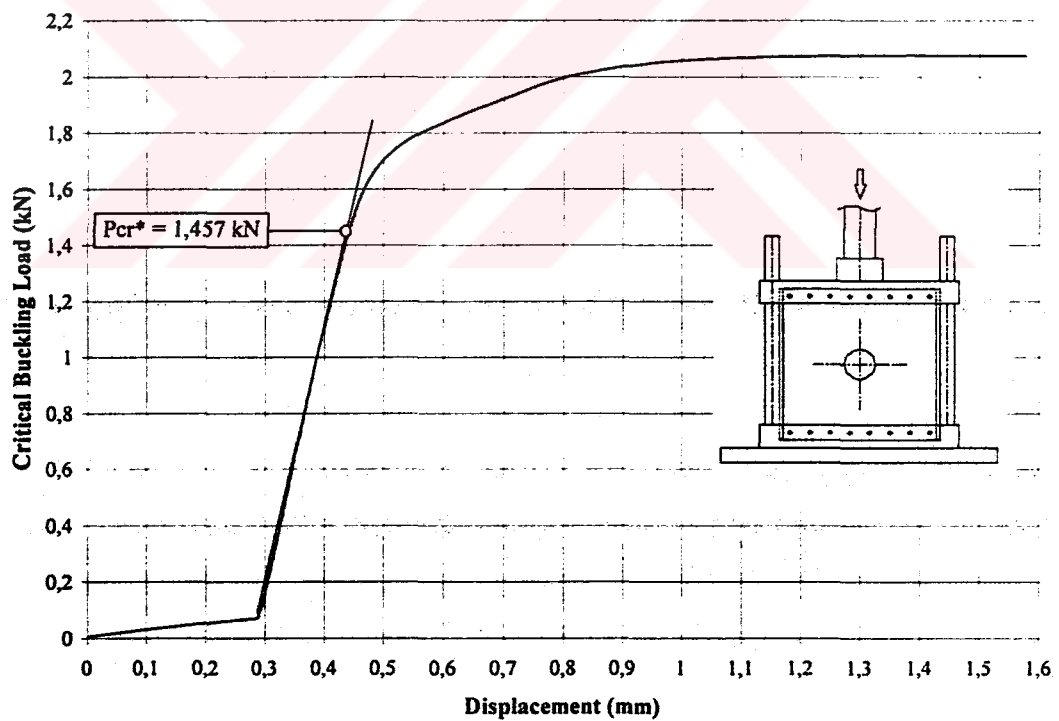


Figure 6.1 Critical buckling load (P_{cr}^*) for the first test specimen without delamination and having 0 degree fiber orientation angle.

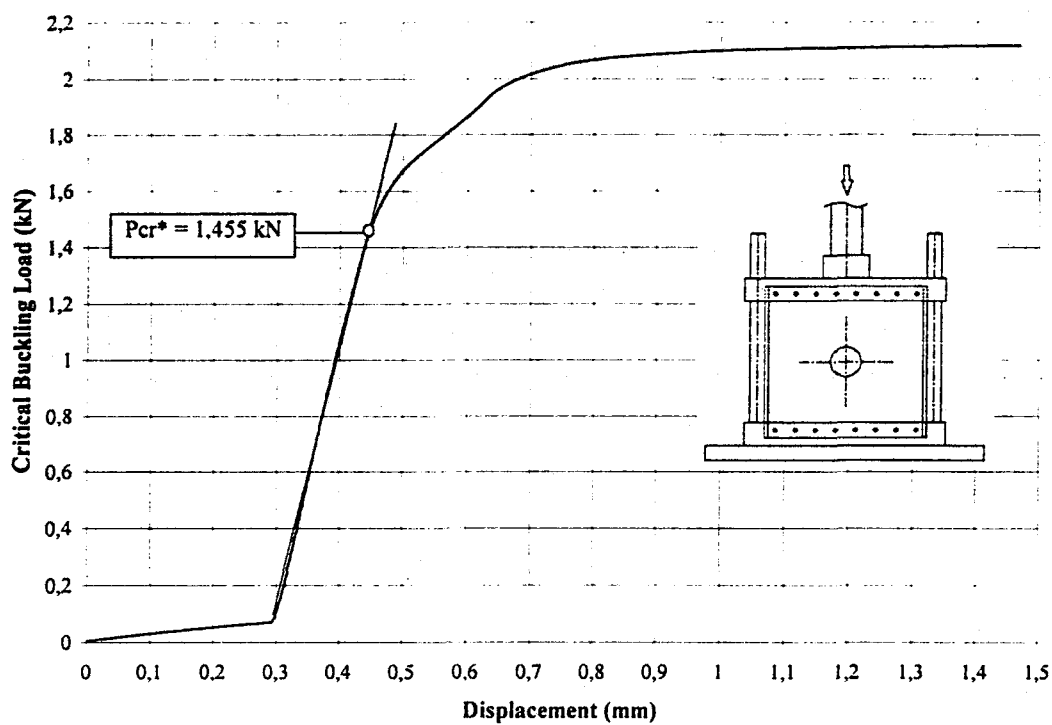


Figure 6.2 Critical buckling load (P_{cr}^*) for the second test specimen without delamination and having 0 degree fiber orientation angle.

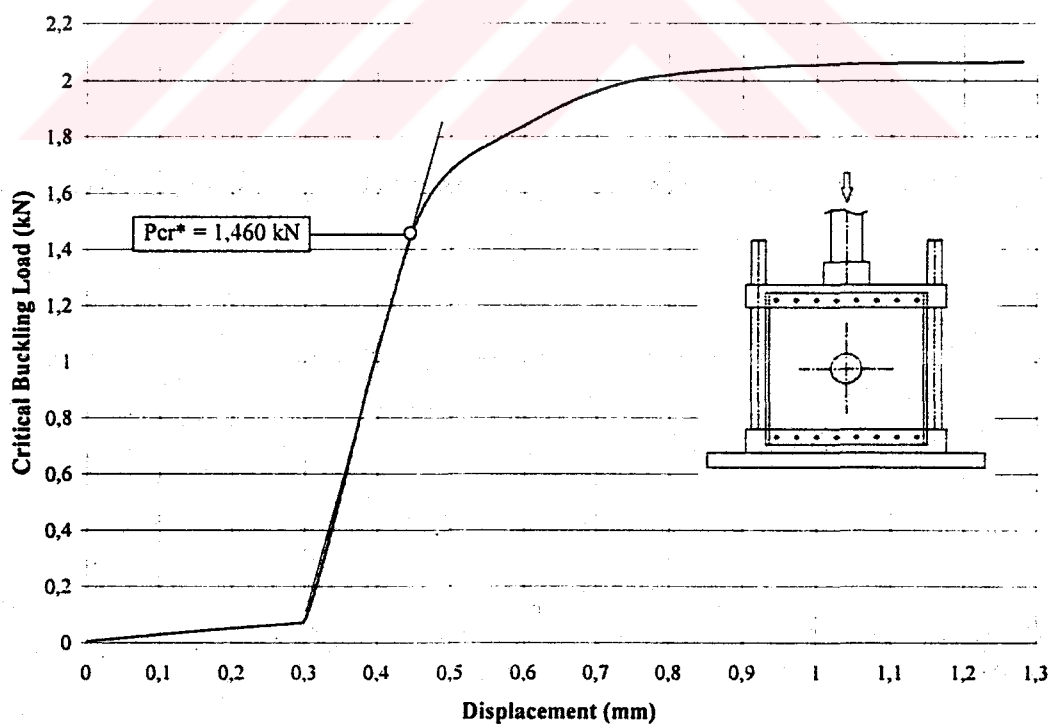


Figure 6.3 Critical buckling load (P_{cr}^*) for the third test specimen without delamination and having 0 degree fiber orientation angle.

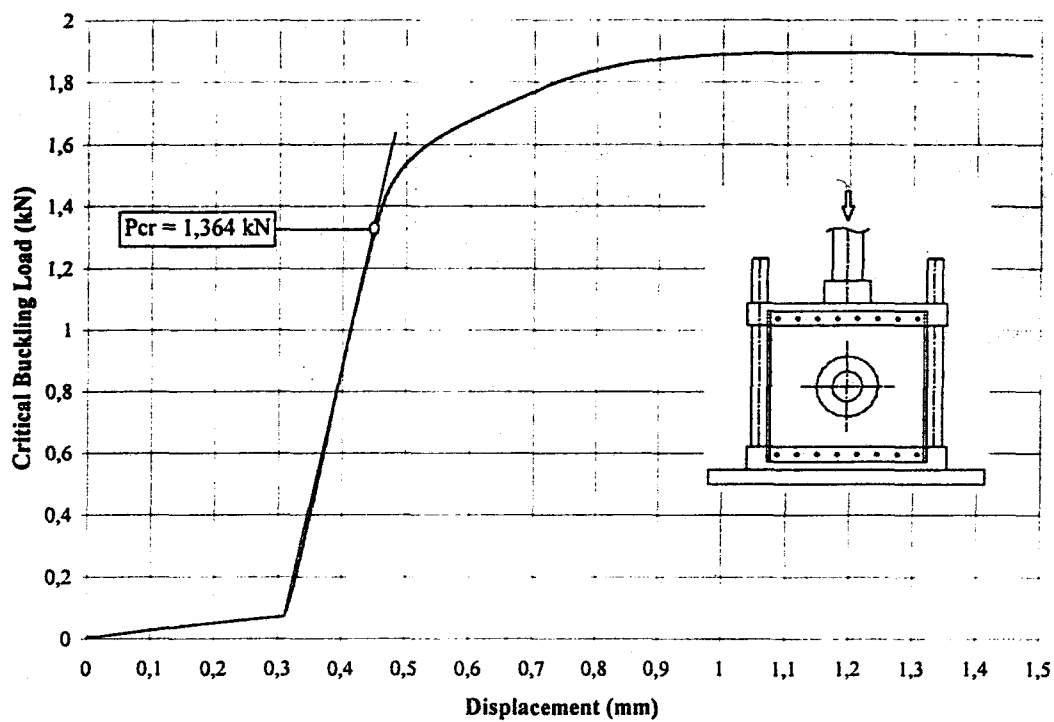


Figure 6.4 Critical buckling load (P_{cr}) for the first test specimen which has 80 mm delamination and 0 degree fiber orientation angle.

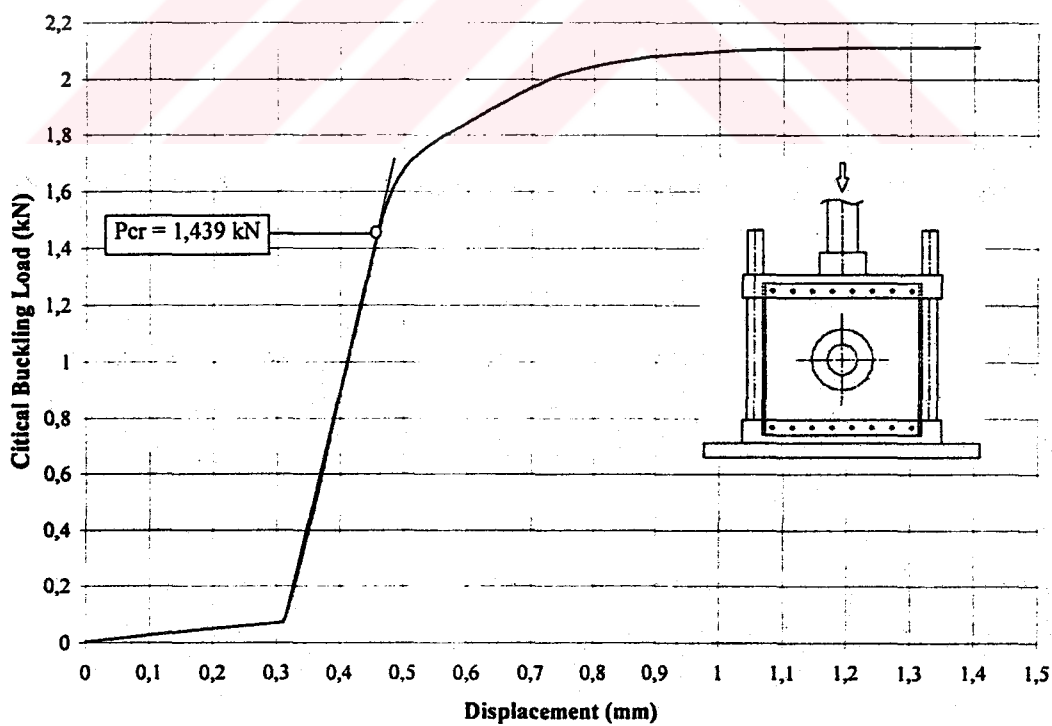


Figure 6.5 Critical buckling load (P_{cr}) for the second test specimen which has 80 mm delamination and 0 degree fiber orientation angle.

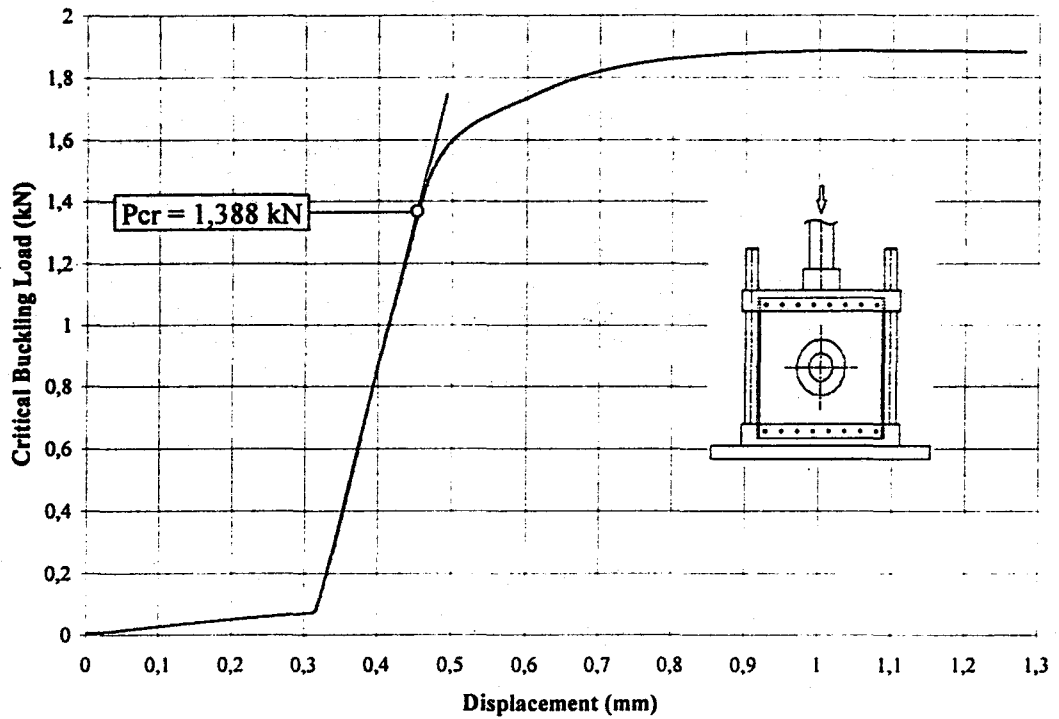


Figure 6.6 Critical buckling load (P_{cr}) for the third test specimen which has 80 mm delamination and 0 degree fiber orientation angle.

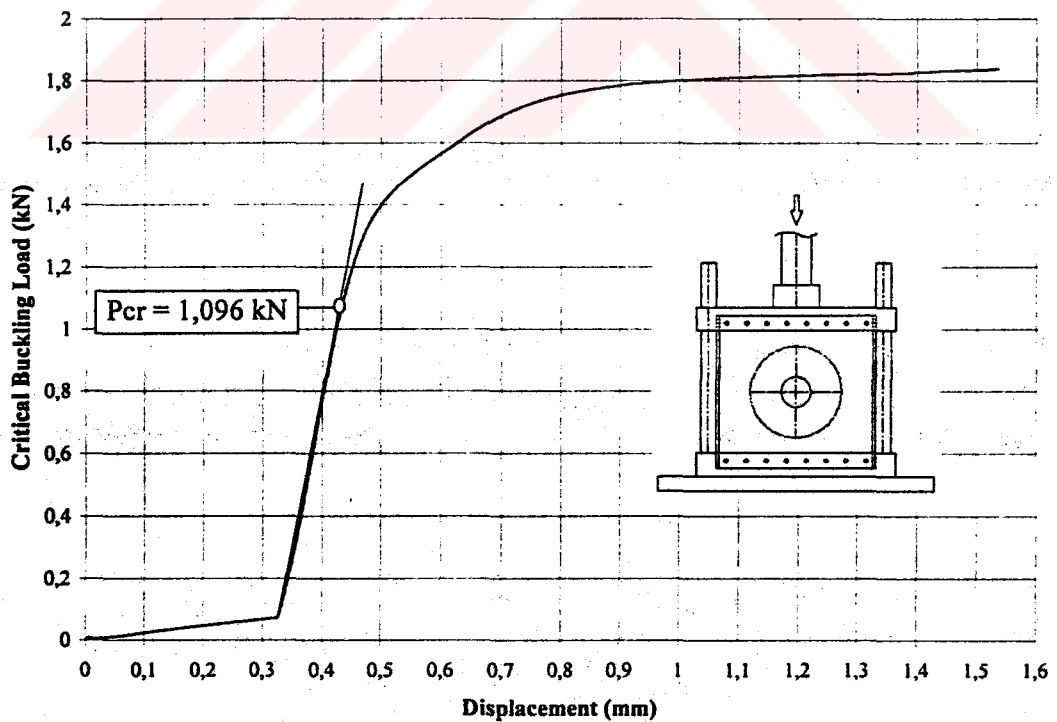


Figure 6.7 Critical buckling load (P_{cr}) for the first test specimen which has 120 mm delamination and 0 degree fiber orientation angle.

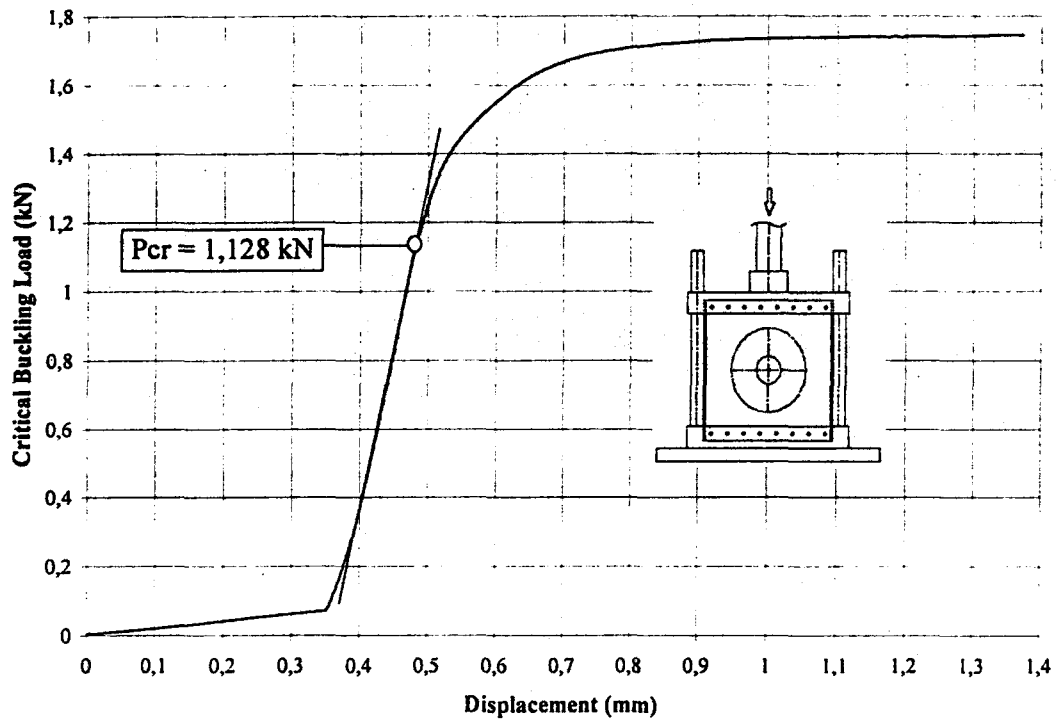


Figure 6.8 Critical buckling load (P_{cr}) for the second test specimen which has 120 mm delamination and 0 degree fiber orientation angle.

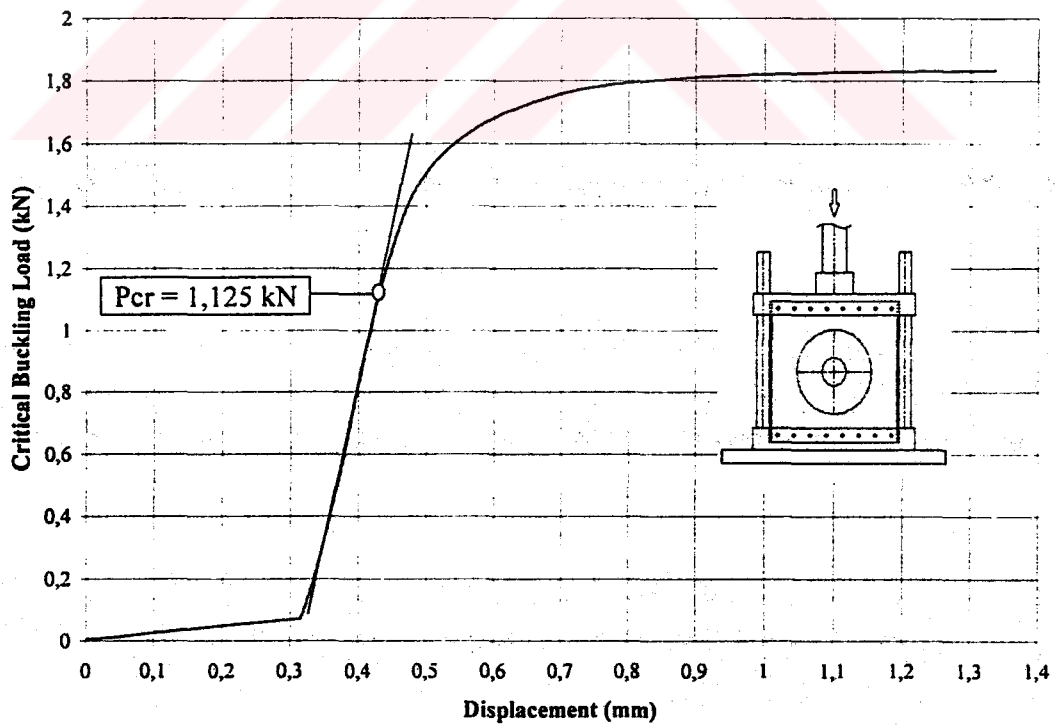


Figure 6.9 Critical buckling load (P_{cr}) for the third test specimen which has 120 mm delamination and 0 degree fiber orientation angle.

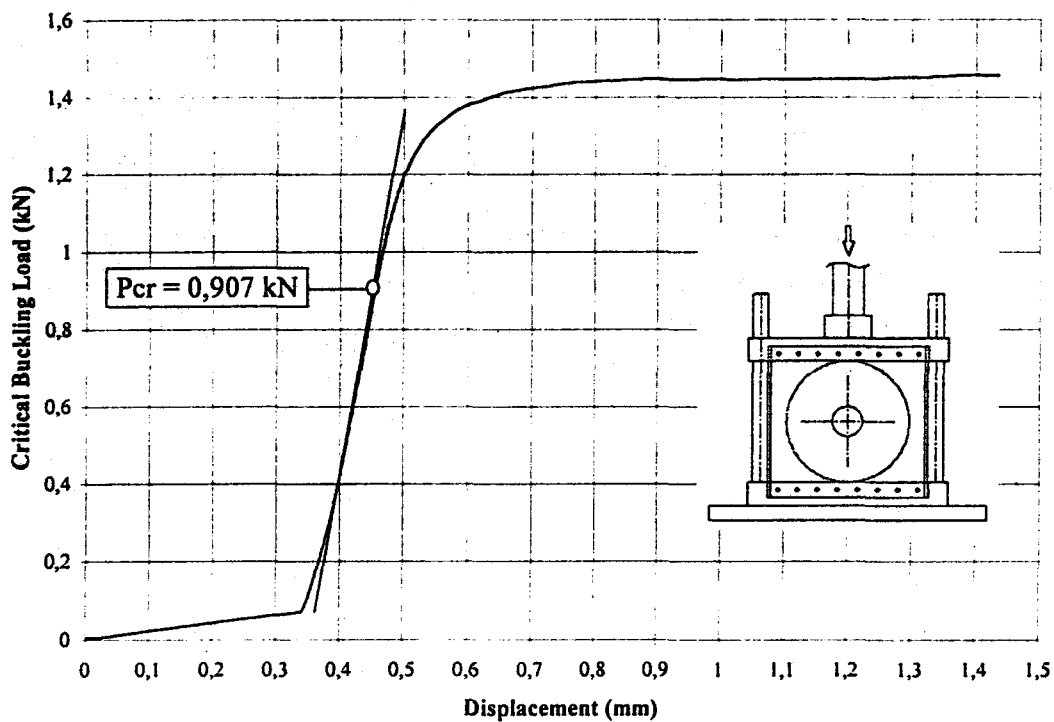


Figure 6.10 Critical buckling load (P_{cr}) for the first test specimen which has 160 mm delamination and 0 degree fiber orientation angle.

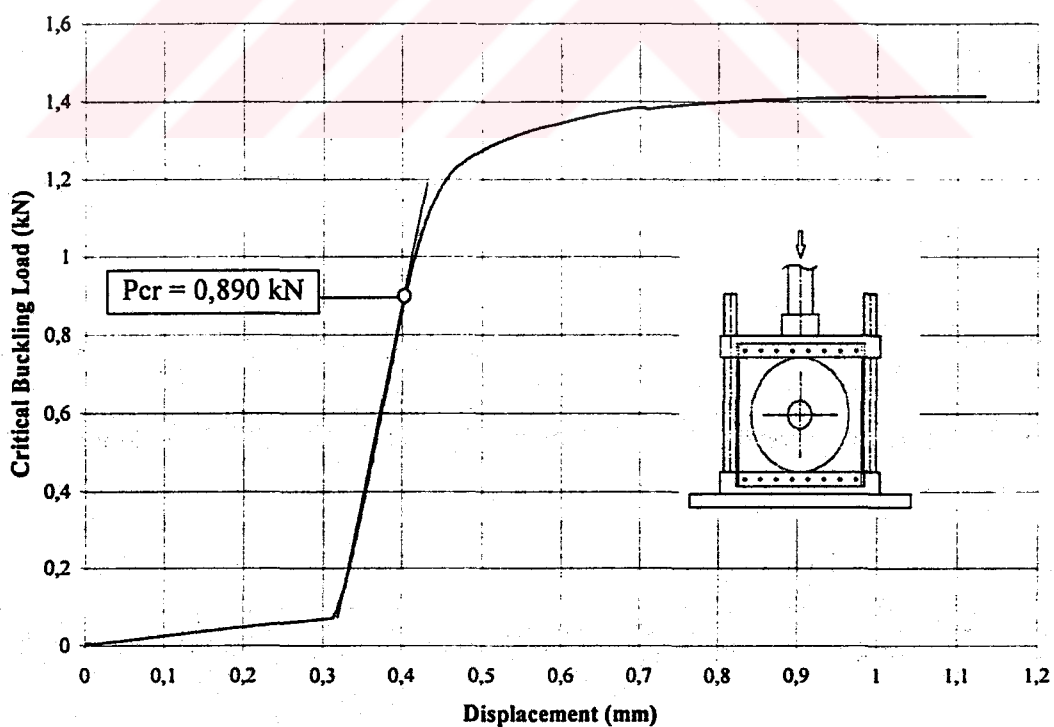


Figure 6.11 Critical buckling load (P_{cr}) for the second test specimen which has 160 mm delamination and 0 degree fiber orientation angle.

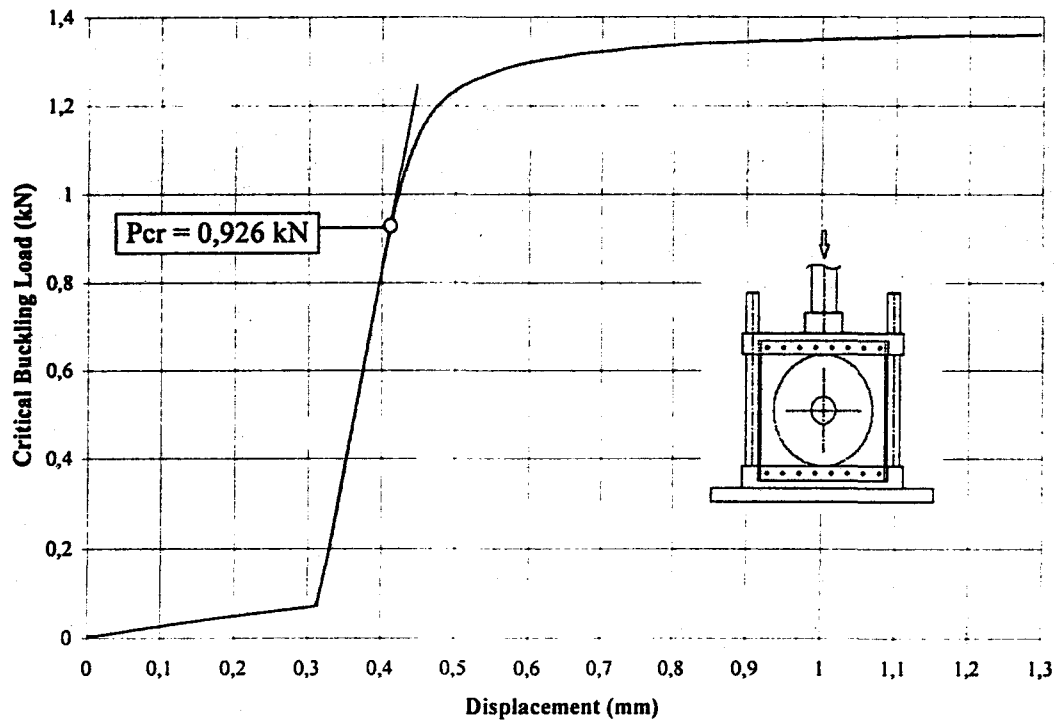


Figure 6.12 Critical buckling load (P_{cr}) for the third test specimen which has 160 mm delamination and 0 degree fiber orientation angle.

Table 6.1 Critical buckling loads and average critical buckling loads for the experimental studies.

		Critical Buckling Loads (P_{cr} , P_{cr}^*) (kN)			
Delamination Diameter (\varnothing_2) (mm)		Test Specimen 1	Test Specimen 2	Test Specimen 3	Average
0	P_{cr}^*	1.457	1.455	1.460	1.458
80	P_{cr}	1.364	1.439	1.388	1.397
120	P_{cr}	1.096	1.128	1.125	1.117
160	P_{cr}	0.907	0.890	0.926	0.908

where, $\varnothing_2 = 0$ has been called as the test specimen without delamination and P_{cr}^* has been called as the critical buckling load in condition without delamination.

From the all experimental results, figures (between Figure 6.1 and Figure 6.12) and Table 6.1, the variation of the critical buckling load with respect to the delamination size has been given in Figure 6.13.

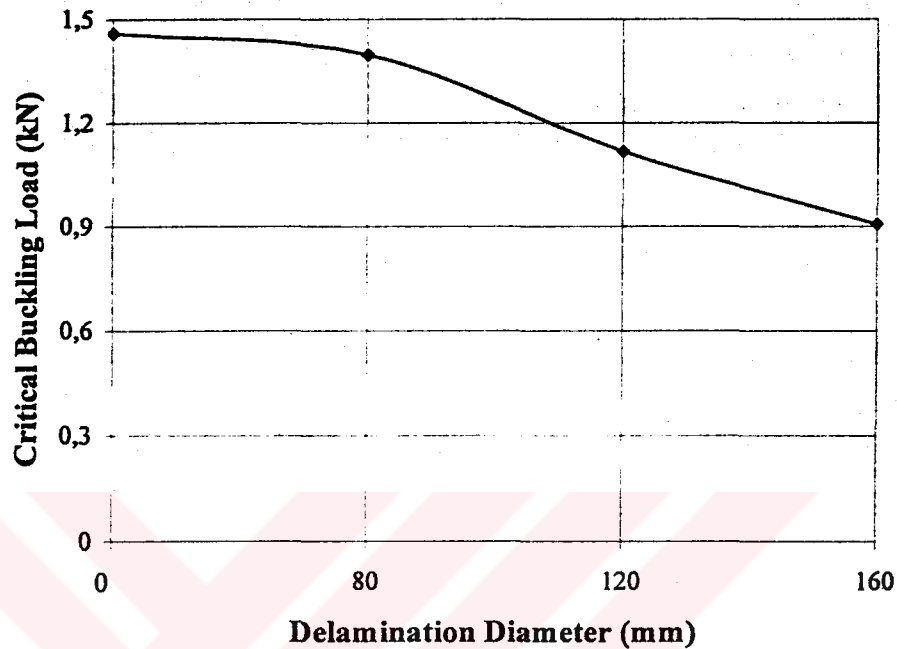


Figure 6.13 Changing of the critical buckling loads with the delamination diameter.

In the Figure 6.13, it is seen that changing of the critical buckling loads according to the delamination diameter. According to this graphic, approximately until $\varnothing_2=60$ mm delamination diameter, the critical buckling load has been shown too small changes and after the $\varnothing_2=60$ mm delamination diameter, this change increased. When the delamination diameter is $\varnothing_2=160$ mm, the critical buckling load has been decreased quite.

Thus, if the delamination diameter (\varnothing_2) approaches to the critical delamination diameter, the critical buckling load doesn't change until a certain value of the delamination diameter, after from this values, the critical buckling load quickly decreases.

In the numerical results, the critical buckling loads have been obtained for the different delamination diameters and different fiber orientation angles. Firstly, for the comparison of the experimental and numerical results, the critical buckling loads of the test specimens which were used in the experiments have been obtained numerically. The numerical results which were obtained with assistance of ANSYS 6.1 finite element analysis program have been given in Table 6.2 and Figure 6.14.

Table 6.2 Critical buckling loads for the numerical studies.

Delamination Diameter (\varnothing_2) (mm)	Critical Buckling Loads (P_{cr} , P_{cr}^*) (kN)	
0	P_{cr}^*	1.457
80	P_{cr}	1.365
120	P_{cr}	1.119
160	P_{cr}	0.835

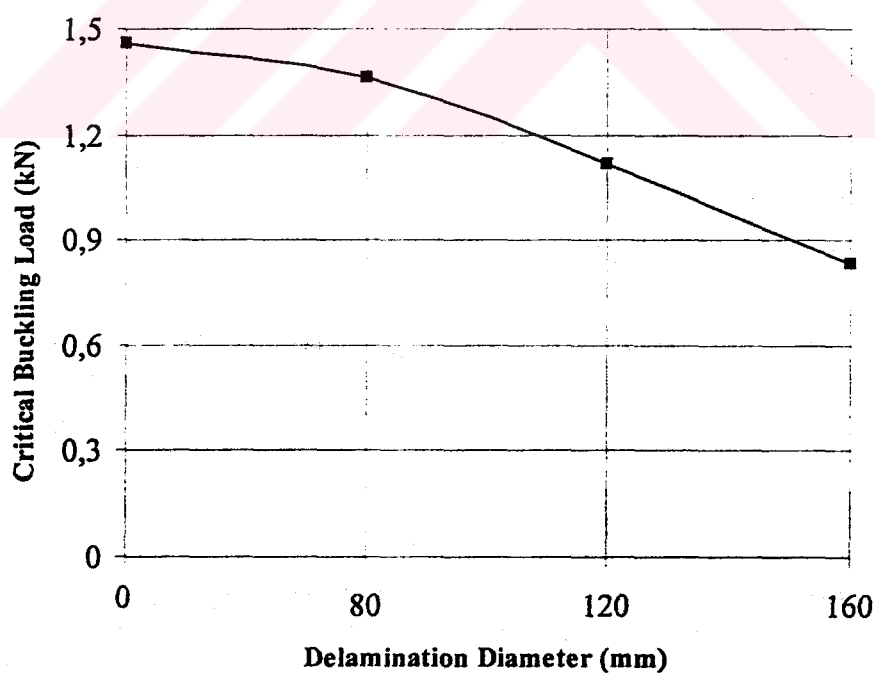


Figure 6.14 Changing of the critical buckling loads with the delamination diameter.

Comparison of the experimental and numerical results has been given in Table 6.3 and Figure 6.15.

Table 6.3 Comparison of the experimental and numerical results.

Delamination Diameter (ϕ_2) (mm)		Critical Buckling Loads (P_{cr} , P_{cr}^*) (kN)	
		Experimental	Numerical
0 (without delamination)	P_{cr}^*	1.458	1.457
80	P_{cr}	1.397	1.365
120	P_{cr}	1.117	1.119
160	P_{cr}	0.908	0.835

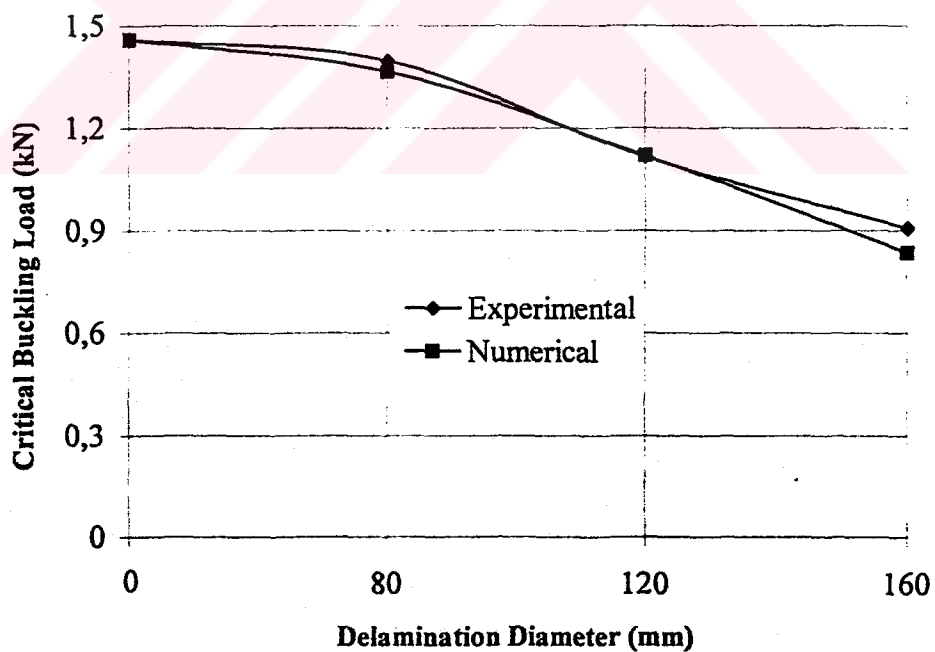


Figure 6.15 Graphical comparison of the experimental and numerical results.

According to Table 6.3 and Figure 6.15, if the delamination diameter approaches to 160 mm, the critical buckling load decreases. Also a good agreement between experimental and numerical results has been found.

After from this comparison between experimental and numerical results, the numerical results have been obtained for the other delamination diameters and fiber orientation angles. All of the numerical results which were obtained have been given in Table 6.4 and Figure 6.16.

Table 6.4 Critical buckling loads for all numerical studies.

Delamination Diameter (\varnothing_2) (mm)		Critical Buckling Loads (P_{cr} , P_{cr}^*) (kN)			
		Fiber Orientation Angles ($^\circ$)			
		$[0^\circ]_s$	$[15^\circ]_s$	$[30^\circ]_s$	$[45^\circ]_s$
0 (without delamination)	P_{cr}^*	1.457	1.395	1.271	1.209
45	P_{cr}	1.454	1.390	1.265	1.203
50	P_{cr}	1.448	1.384	1.259	1.196
55	P_{cr}	1.440	1.377	1.251	1.188
60	P_{cr}	1.430	1.367	1.242	1.179
65	P_{cr}	1.418	1.355	1.230	1.167
70	P_{cr}	1.403	1.341	1.217	1.154
80	P_{cr}	1.365	1.305	1.184	1.121
100	P_{cr}	1.256	1.202	1.090	1.030
120	P_{cr}	1.119	1.071	0.970	0.916
140	P_{cr}	0.973	0.932	0.844	0.795
160	P_{cr}	0.835	0.800	0.725	0.683

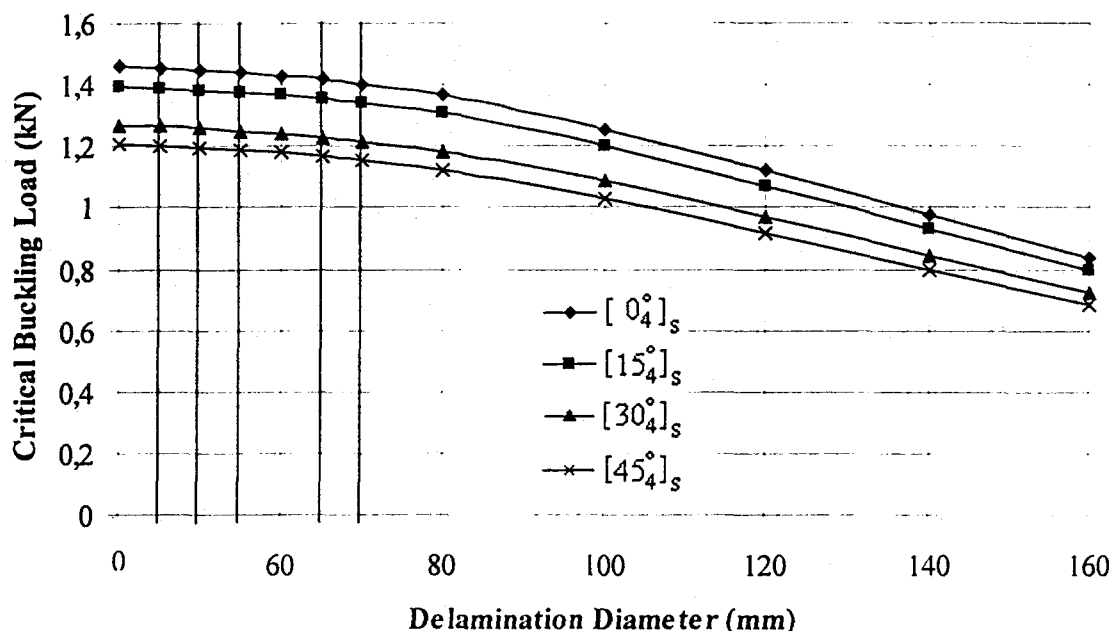


Figure 6.16 Changing of the critical buckling loads according to the delamination diameter.

In the Figure 6.16, variation of the critical buckling loads with the delamination diameter is given. According to this graphic, approximately until $\varnothing_2=60$ mm delamination diameter, the critical buckling load has changed slowly and after the $\varnothing_2=60$ mm delamination diameter, this change has been increased. Also in the numerical results, it has been shown that the critical buckling loads were changed with the fiber orientation angle change. If the fiber orientation angles change as $[0^{\circ}]_s$, $[15^{\circ}]_s$, $[30^{\circ}]_s$, and $[45^{\circ}]_s$, the critical buckling loads decrease.

Finally, it is seen that the different fiber orientation angles affected the critical buckling loads and the important decreases in the critical buckling loads occur after a certain value of the delamination diameter.

CHAPTER SEVEN

CONCLUSION

The effects of the diameter of the circular delamination where exist with regard to circular hole on the buckling behaviour have been investigated experimentally and numerically. In the experimental study, test specimens which have only 0 degree [0°] fiber orientation angle and $\varnothing_2=0\text{mm}$ (without delamination), $\varnothing_2=80\text{mm}$, $\varnothing_2=120\text{mm}$ and $\varnothing_2=160\text{mm}$ delamination diameter have been prepared. In the numerical study, 3D finite element models of the rectangular glass/epoxy laminated composite plates have been established and the effects of the delamination diameter and fiber orientation angle have been investigated with assistance of ANSYS 6.1 finite element analysis program.

From the experimental and numerical results presented it has been concluded that:

1. If the diameter of the circular delamination is smaller than 60 mm which can be called critical delamination diameter, the effects of the delamination diameter and fiber orientation angle on the buckling behaviour can be neglected.
2. The important decreases in the critical buckling loads occur after a certain value of the delamination diameter. After from this delamination diameter, the critical buckling loads decrease quitly, after a short time, if the loading is maintained the critical buckling load can not be changed or the material is deformed.
3. Different fiber orientation angles affect to the critical buckling loads. For example, for the 60 mm delamination diameter, while the critical buckling load is 1.430 kN at the [0°]_s fiber orientation angle, the critical buckling load is 1.367 kN at the [15°]_s fiber orientation angle, 1.242 kN at the [30°]_s fiber orientation angle, 1.179 kN at the [45°]_s fiber orientation angle. It is seen that the critical buckling loads

decrease while fiber orientation angles increase. Similarly, for the other fiber orientation angles it is seen that this changing is similar to the change in the $[0^\circ]_s$ fiber orientation angle. Also, critical buckling behaviours are the same behaviours for the all fiber orientation angles.

4. The delaminations with different shapes, dimensions, numbers and locations among the layers may exist. Their effects on the strength of the materials are clearly different from each other. But the design form of the 3D finite element models used in the present study can be applied on the many problems showing differences due to the delaminations.



REFERENCES

- Kachanov, L. M. (1976). Separation of Composite Materials. Mechanics of Polimers, 5, 918-922.
- Chai, H., Babcock, C. D. and Knauss, W.G. (1981). One-Dimensional Modeling of Failure in Laminated Plates by Delamination Buckling. International Journal of Solids and Structures, 17, 1069-1083.
- Vizzini, A. J. and Lagace, P. A. (1987). The Buckling of A Delaminated Sublaminates on An Elastic Foundation. Journal of Composite Materials, 21, 1106-1117.
- Wang, J. T., Cheng, S. H. and Lin, C. C. (1995). Local Buckling of Delaminated Beams and Plates Using Continous Analysis. Journal of Composite Materials, 29, 1374-1402.
- Wang, S. S., Zahlan, N. M. and Suemasu, H. (1985). Compressive Stability of Delaminated Random Short Fiber Composites Part I-Modeling and Method of Analysis. Journal of Composite Materials, 19, 296-316.
- Wang, S. S., Zahlan, N. M. and Suemasu, H. (1985). Compressive Stability of Delaminated Random Short Fiber Composites Part II-Experimental and Analytical Results. Journal of Composite Materials, 19, 317-333.
- Kutlu, Z. and Chang, F. K. (1992). Modeling Compression Failure of Laminated Composites Containing Multiple Through-Width Delaminations. Journal of Composite Materials, 26, 350-387.
- Adan, M., Sheinman, I. and Altus, E. (1994). Buckling of Multiply Delaminated Beams. Journal of Composite Materials, 28, 77-90.

Chai, H. and Babcock, C. D. (1985). Two-Dimensional Modeling of Compressive Failure in Delaminated Laminates. Journal of Composite Materials, 19, 67-98.

Kassapoglou, C. (1988). Buckling, Post-Buckling and Failure of Elliptical Delaminations in Laminates Under Compression. Composite Structures, 9, 139-159.

Yeh, M. K. and Tan, C. M. (1994). Buckling of Elliptically Delaminated Composite Plates. Journal of Composite Materials, 28, 36-52.

Bottega, W. J. and Maewal, A. (1983). Delamination Buckling and Growth in Laminates, ASME Journal of Applied Mechanics, 50, 184-189.

Hwang, S. F. and Mao, C. P. (1999). The Delamination Buckling of Single-Fiber System and Interply Hybrid Composites. Composite Structures, 46, 279-287.

Zor, M. (2002). Delamination Width Effect on Buckling Loads of Simply Supported Woven-Fabric Laminated Composite Plates Made of Carbon/Epoxy. Journal of Reinforced Plastics and Composites, (In Press).

Jones, R. M. (1999). Mechanics of Composite Materials. (2th ed.). Tokyo: Taylor & Francis.

Chandrupatla, T.R., & Belengundu, A.D. (1991). Introduction to Finite Elements in Engineering. Prentice-Hall.

Moaveni, S. (1999). Finite Element Analysis, Theory and Application with ANSYS. Prentice-Hall.